iScience

CellPress
OPEN ACCESS

Article

p63 and Its Target Follistatin Maintain Salivary Gland Stem/Progenitor Cell Function through TGF-β/Activin Signaling

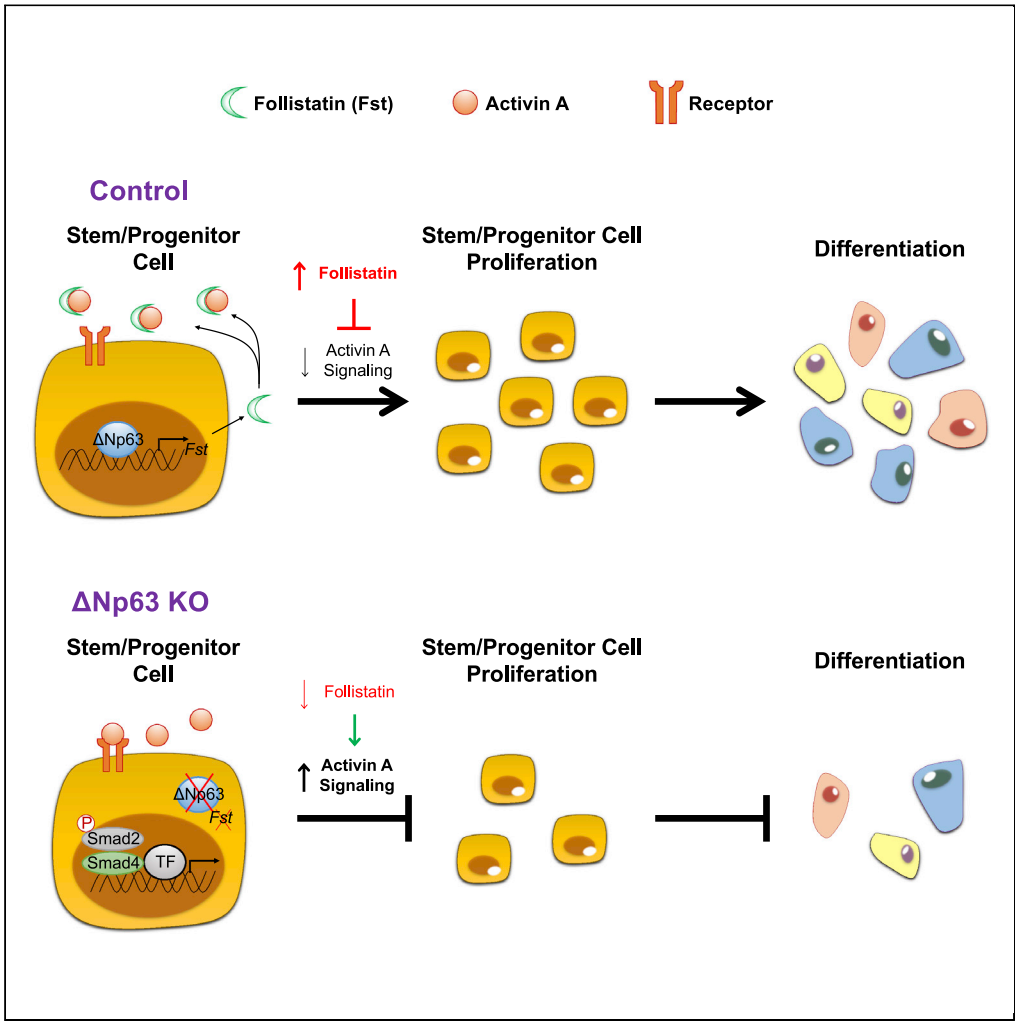

Sangwon Min, Akinsola Oyelakin, Christian Gluck, ..., Elsa Flores, Satrajit Sinha, Rose-Anne Romano

rromano2@buffalo.edu

HIGHLIGHTS

Loss of ΔNp63 expression results in a block in salivary gland cell differentiation

p63 maintains salivary gland stem and progenitor cell proliferation

p63 acts upstream of TGF-β/Activin signaling by directly regulating *Fst* expression

Min et al., iScience *23*, 101524
September 25, 2020
https://doi.org/10.1016/j.isci.2020.101524

iScience

CellPress
OPEN ACCESS

Article

p63 and Its Target Follistatin Maintain Salivary Gland Stem/Progenitor Cell Function through TGF-β/Activin Signaling

Sangwon Min,[1] Akinsola Oyelakin,[1] Christian Gluck,[2] Jonathan E. Bard,[3] Eun-Ah Christine Song,[1] Kirsten Smalley,[1,2] Monika Che,[1] Elsa Flores,[4] Satrajit Sinha,[2] and Rose-Anne Romano[1,2,5,*]

SUMMARY

Multipotent ΔNp63-positive cells maintain all epithelial cell lineages of the embryonic and adult salivary gland (SG). However, the molecular mechanisms by which ΔNp63 regulates stem/progenitor (SP) cell populations in the SG remains elusive. To understand the role of ΔNp63 in directing cell fate choices in this gland, we have generated ΔNp63-deleted adult mice and primary salivary cell cultures to probe alterations in SP cell differentiation and function. In parallel, we have leveraged RNA-seq and ChIP-seq-based characterization of the ΔNp63-driven cistrome and scRNA-seq analysis to molecularly interrogate altered SG cellular identities and differentiation states dependent on ΔNp63. Our studies reveal that ablation of ΔNp63 results in a loss of the SP cell population and skewed differentiation that is mediated by Follistatin-dependent dysregulated TGF-β/Activin signaling. These findings offer new revelations into the SP cell gene regulatory networks that are likely to be relevant for normal or diseased SG states.

INTRODUCTION

Salivary glands (SGs) are exocrine glands whose primary function is to secrete saliva and thereby ensure sufficient lubrication to the oral cavity, which is necessary for proper speech, swallowing, mastication, and digestion of food and for maintaining overall oral health. In humans and rodents, saliva is generated by three major pairs of glands, the parotid (PG), sublingual (SLG), and the submandibular glands (SMG). All three glands share a common structural architecture and comprise secretary units composed of acinar cells, which produce and secrete the saliva into the oral cavity via an intricate and extensive ductal network (Amano et al., 2012). Surrounding the acini and intermingled within the basal cells are myoepithelial cells, a specialized cell type with contractile properties (Tucker, 2007). Irreversible loss of salivary secretion, also known as hyposalivation, is commonly associated with autoimmune diseases such as Sjögren's syndrome, from γ-irradiation therapy used to treat patients with oral cancers, aging, and developmental disorders. Indeed, patients suffering from hyposalivation, which leads to dry mouth, are predisposed to oral infections and have difficulty in speaking, chewing, and swallowing food, all of which can reduce their overall quality of life (Harunaga et al., 2011). Currently, there are no curative treatment options for these patients. This has spurred renewed interest in developing new strategies aimed at restoring SG function using stem cell-based approaches (Pringle et al., 2016; Nanduri et al., 2014). However, our current understanding of the basic physiological mechanisms and the transcriptional networks regulating stem/progenitor (SP) cell self-renewal, proliferation, and differentiation programs in the SG remains elusive.

p63, specifically the ΔNp63 isoform, is a lineage-specific master transcription factor that is highly expressed in epithelial-rich tissues and organs where it is plays important roles in stem cell self-renewal, cell fate decisions and lineage commitment, morphogenesis, and directing differentiation programs (Romano et al., 2012; Fan et al., 2018; Chakravarti et al., 2014; Chakrabarti et al., 2014; Senoo et al., 2007; Packard et al., 2011; Blanpain and Fuchs, 2007; Kumar et al., 2019). Interestingly, these studies have unearthed important p63-driven signaling pathways that direct stem cell fate choices in various stratified epithelial tissues and glandular secretory organs. Indeed, p63 has been shown to act upstream of a number of key signaling pathways including Wnt, Notch, and Egf in both the skin and mammary gland (Forster et al., 2014; Chakrabarti et al., 2014; Romano et al., 2012; Fan et al., 2018). In the SG, ΔNp63 is expressed in the epithelial cells of the

[1]Department of Oral Biology, State University of New York at Buffalo, School of Dental Medicine, 3435 Main Street, Buffalo, NY 14214, USA

[2]Department of Biochemistry, State University of New York at Buffalo, Buffalo, NY 14203, USA

[3]Genomics and Bioinformatics Core, State University of New York at Buffalo, Buffalo, NY 14203, USA

[4]Department of Molecular Oncology, H. Lee Moffitt Cancer Center and Research Institute, Tampa, FL 33612, USA

[5]Lead Contact

*Correspondence: rromano2@buffalo.edu

https://doi.org/10.1016/j.isci.2020.101524

developing placode, where it plays a critical role as ΔNp63-null animals display a complete block in gland morphogenesis (Romano et al., 2012). The contribution of ΔNp63 in actively directing SP cell fate choices in the SG is further highlighted by recent genetic lineage tracing studies, which demonstrated that $p63^{+ve}$ cells give rise to and maintain all the epithelial cell lineages in both embryonic and adult glands (Song et al., 2018). Although the role of ΔNp63 in SG development has been established, our understanding of the molecular function of this regulator in directing the intrinsic signals that define SG SP cell identity, self-renewal, maintenance, and differentiation are not well understood.

Transforming growth factor β (TGF-β) superfamily signaling has been implicated in driving developmental programs, cellular proliferation, and differentiation (Wu and Hill, 2009; Massague, 2012). Signaling by this superfamily has also been shown to play a prominent role in directing SP cell fate choices important for tissue homeostasis and regeneration (Lepletier et al., 2019; Mou et al., 2016; Suzuki et al., 2017). TGF-β signaling comprises TGF-β, bone morphogenetic proteins (BMPs), growth and differentiation factors (GDFs), Activins, Nodal, and anti-Mullerian hormone (AMH) (Oshimori and Fuchs, 2012). Activins, considered evolutionarily to be the most ancient of the TGF-β signaling family members, signal through the type II Activin receptors and exert their function through the downstream effectors, phosphorylated Smad2 and Smad3. Moreover, in stratified epithelia including that of the skin, airway, and mammary gland, TGF-β/BMP/SMAD pathway signaling has been shown to be active in the differentiated luminal and suprabasal cells while being suppressed in the undifferentiated basal cells of these tissues (Mou et al., 2016; Suzuki et al., 2017). Although the role of TGF-β as a multifunctional cytokine that influences branching morphogenesis and extracellular matrix (ECM) deposition in the SG is well established, its role in directing SP cell fate choices and the identity of key upstream transcriptional regulators remains elusive.

To better investigate the function of p63 in directing cell fate choices in the murine submandibular salivary gland (SMG), we have generated animals with targeted deletion of ΔNp63 in adult glands. We demonstrate that ablation of ΔNp63 results in aberrant epithelial differentiation, which is accompanied by a dramatic loss to the SP cell population. To dissect the distinct p63-driven regulatory circuitry through which this transcription factor functions to maintain this important cell type, we have performed transcriptomic (RNA sequencing) and single cell RNA sequencing (scRNA-seq) of ΔNp63-null SGs. Integrated analysis of our transcriptomic studies reveals that ΔNp63 maintains the proliferative capacity and differentiation potential of SG epithelial SP cells by regulating TGF-β signaling. Moreover, by combining our transcriptomic and epigenomic (ChIP-seq) studies, we find that ΔNp63 directly regulates the expression of *Follistatin*, a key modulator of the Activin/SMAD signaling network, to maintain the proliferative state of SG SP cells. Taken together, our data demonstrate that the transcription factor ΔNp63 functions as an upstream regulator of the TGF-β signaling pathway governing the proliferative and differentiation programs in SG epithelial SP cells.

RESULTS

ΔNp63 Deletion Results in Alterations to the Salivary Gland Epithelial Cell Differentiation Program

In the SG, ΔNp63 expression is restricted to the basal and myoepithelial cells where $\Delta Np63^{+ve}$ cells have been shown to give rise to and maintain all the epithelial cell lineages in embryonic and adult glands (Song et al., 2018). To examine the role of ΔNp63 in adult SG maintenance, we crossed $\Delta Np63^{fl/fl}$ mice to a transgenic strain that ubiquitously expresses Cre-recombinase fused to the estrogen-ligand binding domain ERT2 ($UBC^{CreERT2}$). This inducible conditional mouse model system allowed for overcoming the perinatal lethality associated with loss of p63 and also for the excision of $\Delta Np63$ in both the basal and myoepithelial cell populations as shown in other organs such as the skin and mammary glands (Kumar et al., 2019; Chakravarti et al., 2014). Tamoxifen (TAM) was administered to adult $\Delta Np63^{fl/fl}$ (control) and $UBC^{CreERT2}$; $\Delta Np63^{fl/fl}$ (ΔNp63KO) mice, and SGs were harvested 8–10 days post TAM administration and analyzed. This time line was chosen since the ΔNp63KO animals appeared slightly smaller and leaner and exhibited some hair loss compared with control mice (Figure 1A). Loss of ΔNp63 expression in the SG was verified at both the protein and mRNA levels (Figures 1B and 1C). We next assessed for gross effects of the loss of $\Delta Np63$ on the SMG by measuring salivary gland weight. Interestingly, we found a reduction in the weights of both male and female knockout glands compared with the controls (Figure 1D). Histological analysis of hematoxylin and eosin (H&E)-stained paraffin-embedded SMGs in both male and female mice revealed a dramatic reduction in ductal size in the SMGs of ΔNp63KO mice when compared with control and ΔNp63 heterozygous (ΔNp63Het) animals (Figures 1E and S1A). The observed phenotype in the ducts

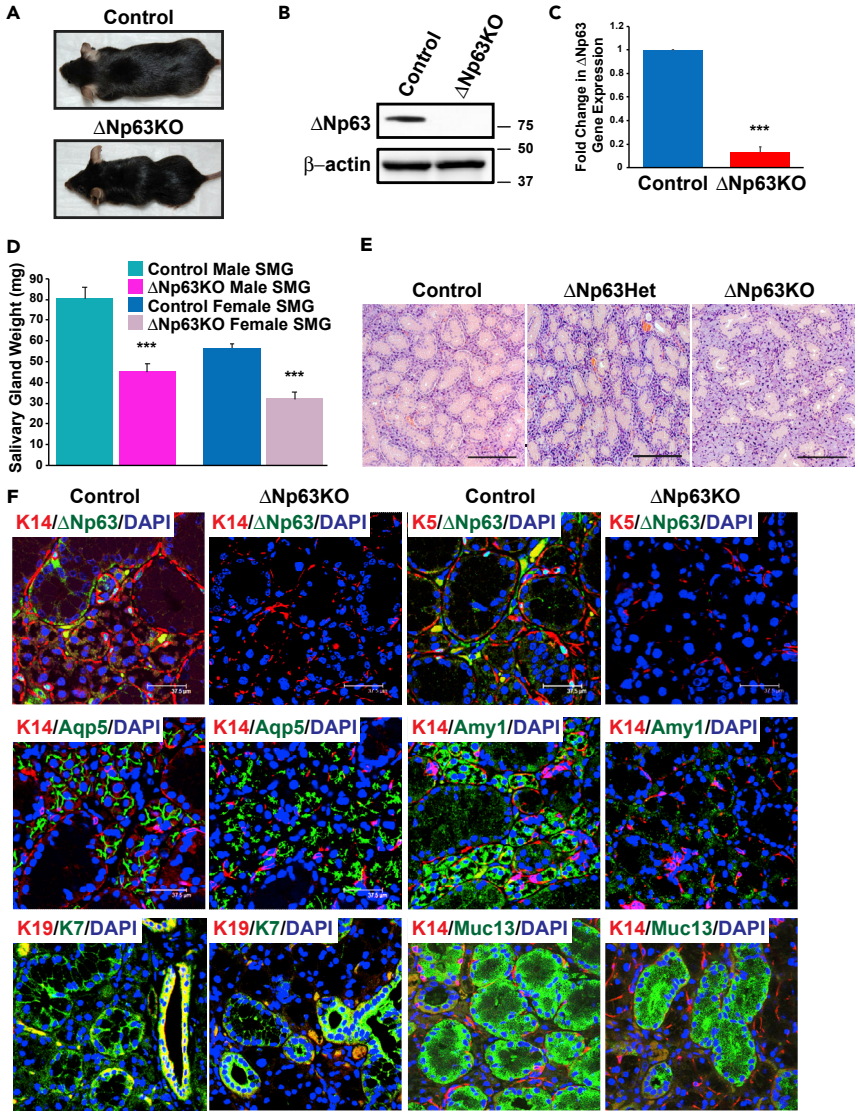

Figure 1. Histological and Immunochemical Analysis of Submandibular Salivary Glands of Mice with Targeted Deletion of ΔNp63

(A) Gross morphology of ΔNp63KO and control animals.

(B) Western blot analysis demonstrates reduced protein expression levels of ΔNp63 in SMGs of ΔNp63KO mice compared with controls.

(C) Quantitative RT-PCR analysis showing ΔNp63 mRNA expression levels in the SMGs of control and KO mice.

(D) Weight of submandibular salivary glands from control and ΔNp63KO male and female mice.

(E) H&E staining of control, ΔNp63 heterozygous (ΔNp63Het), and ΔNp63KO male SMGs. Compared with control and ΔNp63Het glands, KO mice show reduced ductal size along with enlarged acini. Scale bar: 200 μm.

(F) Immunofluorescence staining of male control and ΔNp63KO glands confirm the loss of ΔNp63 expression as well as a dramatic reduction in the K5 and K14 stem/progenitor cell population. Alterations to the acinar cell differentiation program is also observed in the KO glands as evident by the loss of Amy1 expression. K7 and Muc13 expression levels appear unchanged in the ducts of the mutant glands, whereas K19 expression is reduced. Scale bar: 37.5μm.

Data are represented as mean ± SD (n = 3). ***$p < 0.001$. See also Figures S1–S4.

was accompanied by alterations to the acinar cells, which appeared enlarged in the ΔNp63KO as compared with control and ΔNp63Het mice (Figures 1E and S1A). Indeed, further quantification analysis comparing the duct and acini cell areas confirmed our findings (Figures S2A and S2B). To better define the overall cellular nature of the phenotypic changes resulting from the loss of ΔNp63, we performed immunofluorescence studies and examined both male and female KO SMGs utilizing a battery of well-

established epithelial cell markers. Evaluation of the progenitor cell markers Keratin 5 (K5) and K14, which are restricted to the basal and myoepithelial cell populations in control mice, revealed a dramatic reduction in protein expression levels in SMGs of the ΔNp63KO mice, suggesting a loss to the progenitor cell populations (Figures 1F and S1B). In addition, in the ΔNp63KO mice, we observed reduced protein expression levels of α-smooth muscle actin (Sma), which is primarily expressed in the myoepithelial cells of the SG (Figures S3A and S3B). In agreement with our histological analysis, we observed reduced expression levels of the water channel protein aquaporin 5 (Aqp5) and the salivary enzyme amylase 1 (Amy1), in the ΔNp63KO glands compared with the control (Figures 1F and S1B). Interestingly, we did not observe any differences in the expression of $Na^+/K^+/2Cl^-$ co-transporter (Nkcc1), mucin10 (Muc10), or the transcription factor Mist1, all of which are specifically and uniquely enriched in the acinar cells (Figures S3A and S3B). Similarly, we did not detect alterations to the expression pattern of the granular convoluted ductal markers mucin13 (Muc13) or K7 in the glands of the ΔNp63KO mice (Figures 1F and S1B) (Amano et al., 2012). However, K19 expression, which is typically localized to the striated and excretory ducts, was dramatically reduced in the mutant glands compared with the control (Figures 1F and S1B). Since our immunofluorescence analysis did not reveal any significant alterations to the ductal cell differentiation program that could account for the dramatic decrease in overall duct size and individual ductal cell size in the ΔNp63KO mice (Figures 1F, S1B, S2, and S4A), we assessed whether these changes were driven by proliferation defects. Although the KO glands revealed a modest reduction in proliferation based on expression of the proliferation marker Ki67, we did observe a significant increase in apoptosis as demonstrated by the elevated numbers of ductal cells that stained positive for the apoptosis marker cleaved caspase-3 (Casp3) as compared with control glands (Figures S4B and S4C). Interestingly, this was accompanied by reduced salivary production in the KO glands (Figure S4D). As expected, we did not detect expression of ΔNp63 in the SMGs of the KO mice, confirming deletion of the ΔNp63 allele (Figure S1 and S3). To confirm our findings in an independent mouse model system, and to ensure that the phenotype we observed was not due to the broad effects of UBC-Cre-ERT2, inefficient Cre-mediated recombination, or secondary effects resulting from the global loss of ΔNp63, we crossed $\Delta Np63^{fl/fl}$ mice to a transgenic strain expressing Cre-ERT2 under the control of the *Trp63* ($Trp63^{CreERT2}$) gene locus (Lee et al., 2014). Analogous to the phenotype observed in the $UBC^{CreERT2};\Delta Np63^{fl/fl}$ KO mice, the $Trp63^{CreERT2};\Delta Np63^{fl/fl}$ KO animals demonstrated similar histological and cellular alterations to the SG differentiation program (Figure S3C). Given that two independently generated ΔNp63KO strains displayed similar phenotypes regardless of sex, all subsequent studies were performed with $UBC^{CreERT2};\Delta Np63^{fl/fl}$ animals.

Perturbations in Transcriptional and Signaling Networks upon the Loss of ΔNp63

To probe the effects of the loss of ΔNp63 in adult SGs, next we compared the transcriptomic profiles of the control and ΔNp63KO SMGs by RNA-seq. Our analysis identified ~2,800 differentially expressed genes (DEGs) between the control and KO glands, with 1,285 genes upregulated and 1,555 genes showing downregulation (Figure 2A and Table S1). Gene ontology analysis of the DEGs revealed enrichment of genes associated with Regulation of Signaling, Programmed Cell Death, and Cell Cycle (Figure 2B). In contrast, downregulated genes were associated with Epithelial Cell Proliferation, Cell Differentiation, and Stem Cell Population Maintenance (Figure 2C). Indeed, genes commonly associated with SP cell function were downregulated, as were genes involved in SG differentiation and salivary secretion (Figure 2D). Moreover, crucial players involved in the TGF-β, Notch, MAPK, Hippo, and Wnt signaling were also significantly altered upon the loss of ΔNp63 (Figure 2D). These findings are in line with other studies of gene expression changes that are unleashed upon the loss of p63 (Fan et al., 2018; Chakrabarti et al., 2014; Romano et al., 2012). We further confirmed the expression of a subset of key genes that were altered upon the loss of ΔNp63 expression by quantitative reverse-transcriptase polymerase chain reaction (qRT-PCR), thereby validating our RNA-seq results (Figure 2E). Taken together, these results reveal the global changes in the transcriptome, as well as alterations to various signaling pathways accompanying the loss of ΔNp63 in SMGs.

ΔNp63 Maintains Stem/Progenitor Cell Activity

Given that our transcriptomic analysis revealed downregulation of genes involved in stem cell biology in the KO glands compared with the control, we next sought to explore the functional importance of ΔNp63 in SP cell activity. Indeed, mining of our RNA-seq datasets revealed downregulation of a number of well-established SG SP cell markers (Figure 3A) (Pringle et al., 2013). To further investigate the status of the SP cell populations, we performed fluorescence-activated cell sorting (FACS). As expected, our FACS analysis revealed a dramatic loss to the $CD24^{hi}/CD29^{hi}$ SP cell population (Figure 3B) in the ΔNp63KO glands compared with the control animals

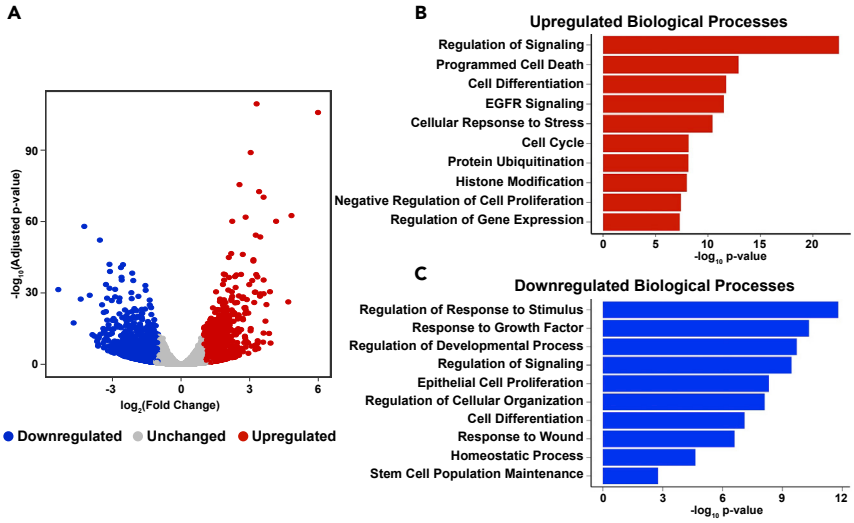

D

Stem/Progenitor Genes	Kit(-1.08), Krt14(-2.59), Krt5(-2.10), Sox10(1.19),Trp63(-1.07)
Differentiation	Krt18(1.27), Krt19(-1.87), Myl9(-1.19), Acta2(-1.02)
Salivary Secretion	Adcy7(-1.08), Adcy8(-1.50), Atp1b2(-1.14), Calm(-1.45), Calm3(1.11), Calml3(-1.02), Kcnma1(1.49), Nos(-1.86), Prb(1.29)
TGF-β Signaling	Acvrb(1.39), Bmp4(1.75), Crebbp(1.09), Smurf(1.33), Tgfb2(-2.63), Tgfb3(-1.18), Tgif1(1.11), Thbs(-1.46), Zfyve16(-1.40), Fst(-1.10)
Notch Signaling	Dll1(-1.31), Dvl1(1.29), Jag2(-1.20), Lfng(-1.33), Ctbp2(-1.05)
MAPK Signaling	Egf(-2.41), Elk4(1.29), Fgf1(-1.70), Fgf9(-2.88), Fgfr2(2.03), Fos(1.65), Jund(1.28), Mapk2k5(1.11), Mapk3k6(2.26), Mapk3k8(1.85), Ngf(-3.04), Akt3(-1.21)
Hippo Signaling	Csnk1e(1.13), Id2(-1.85), Llgl2(1.66), Nkd1(-2.41), Ppp2r2c(-1.54), Serpine1(-1.70), Snai2(-2.04), Gdf5(-1.17)
Wnt Signaling	Ctbp2(-1.05), Fzd5(2.29), Fzd6(1.24), Fzd9(1.09), Nfatc1(1.16), Wnt2b(1.05), Wnt9a(2.15), Dvl2(1.29)

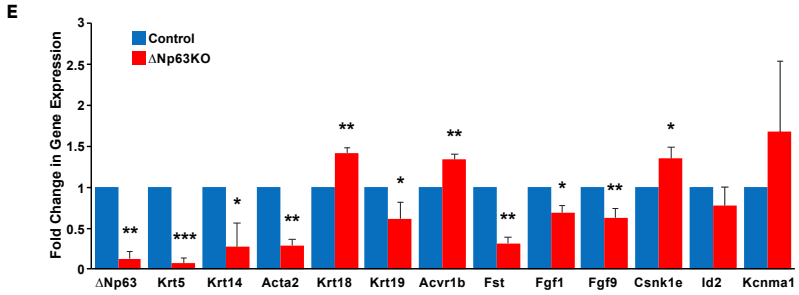

Figure 2. ΔNp63-Driven Transcriptomic Changes in the Adult Salivary Gland

(A–C) (A) Volcano plot shows the distribution of statistically significant DEGs in the SMG upon deletion of ΔNp63. Upregulated genes are depicted in red and downregulated genes are shown in blue. Bar plots highlighting the top enriched upregulated (B) and downregulated (C) biological processes.

(D) Transcriptomic changes in control as compared with ΔNp63KO SMG. Red indicates upregulated genes and blue represents downregulated genes.

(E) Quantitative RT-PCR validation of selected genes in control and ΔNp63KO SMGs. Values were normalized to the housekeeping gene *Hprt*. Data are represented as mean ± SD (n = 3).*p < 0.05, **p < 0.01, ***p < 0.001.

See also Figure S6 and Table S1.

(Nanduri et al., 2011, 2014). We next sought to examine the function of ΔNp63 in maintaining the clonogenic properties in salivary gland epithelial progenitor cells. In order to address this, we first established a system to support the clonal growth of salivary gland epithelial progenitor cells. Toward this end, primary salivary gland epithelial cells isolated from adult wild-type mice were grown in CnT-PR media, a commercially available basal media commonly used to grow progenitor cells from diverse epithelial tissues (Suzuki et al., 2017). Indeed, we found that, after 2 weeks of culture, primary salivary gland epithelial cells readily formed clones (Figure 3C). Importantly, a large percentage of the cells within the epithelial clones expressed high levels of ΔNp63 despite being derived from adult salivary glands in which only 5%–6% of the total epithelial cells are $\Delta Np63^{+ve}$ (Figure 3C) (Song et al., 2018). Having established this clonogenic assay for primary salivary gland epithelial progenitor cells (pSEPCs) we next investigated the effects of loss of ΔNp63 on clonogenic potential. Toward this end, pSEPCs

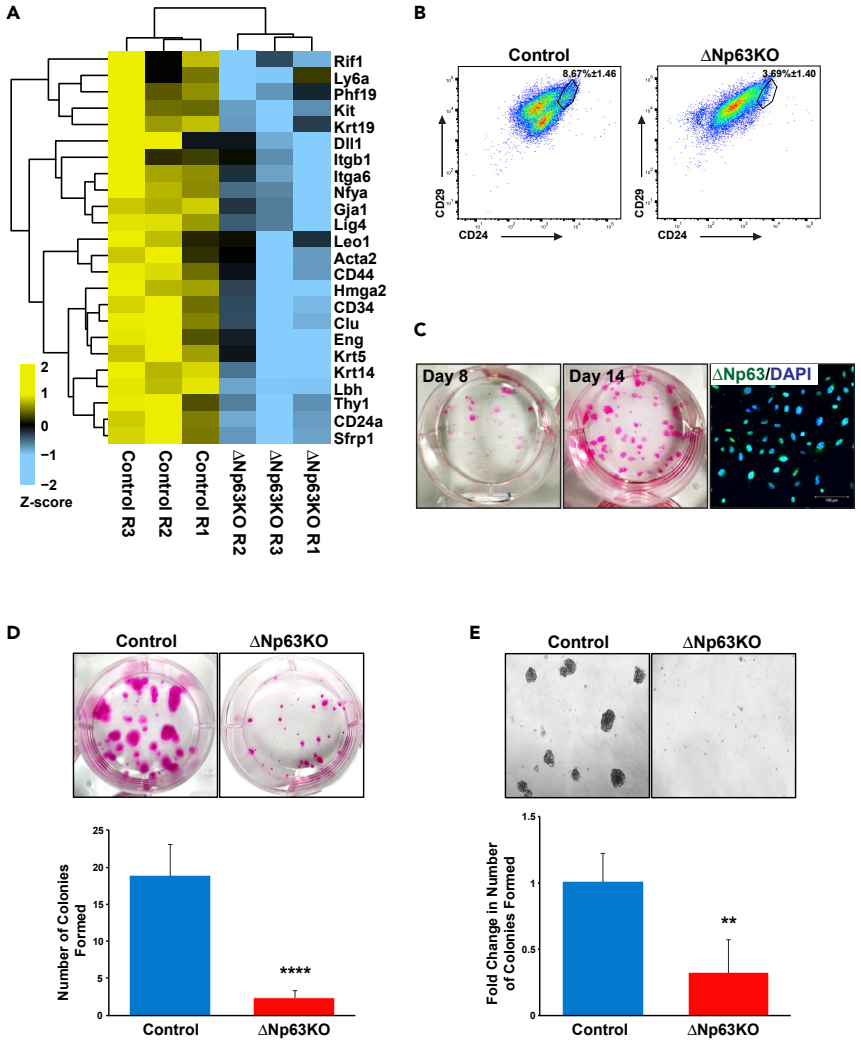

Figure 3. ΔNp63 Maintains the Proliferative Potential of Salivary Gland Epithelial Progenitor Cells

(A) Heatmap visualization of selected DEGs corresponding to a panel of well-established salivary gland stem/progenitor cell markers in control and KO SMGs (Pringle et al., 2013).

(B) Representative FACs profiles of $CD24^{hi}/CD29^{hi}$ SP cells from control and ΔNp63KO mice.

(C) Representative images of Rhodamine B staining of pSEPCs clones grown at indicated time points. Right panel shows 14-day clones stained with an anti-ΔNp63 antibody showing enrichment of $\Delta Np63^{+ve}$ epithelial cells in the clones. Scale bar: 100 μm.

(D) Representative images of Rhodamine B staining of pSEPCs clones grown for 14 days from control and KO animals. Bottom panel is a quantification of the number of colonies formed in control as compared with ΔNp63KO mice.

(E) Representative images of control and ΔNp63KO pSEPCs 3D-spheroids grown on matrigel.

Data are represented as mean ± SD (n = 4). $^{**}p < 0.01$, $^{****}p < 0.0001$.

isolated from control and ΔNp63KO mice were grown in culture and clonal growth was assessed based on the number of colonies formed over time (Suzuki et al., 2017). Indeed, after 14 days we observed a dramatic loss in the clonogenic capabilities of pSEPCs isolated from the ΔNp63KO mice, compared with control animals (Figure 3D). In parallel we also compared the ability of isolated pSEPCs to form colonies as three-dimensional spheroid structures when grown on a 3D Matrigel-based matrix. By day 14, control pSEPCs formed larger salispheres consisting of tightly packed cells, whereas ΔNp63KO cells yielded significantly fewer and smaller sized spheres (Figure 3E). Overall, these results are consistent with a primary role for ΔNp63 in maintaining the proliferative potential of primary salivary gland epithelial progenitor cells, similar to what has been reported in progenitor cells from other epithelial tissues (Senoo et al., 2007; Chakrabarti et al., 2014).

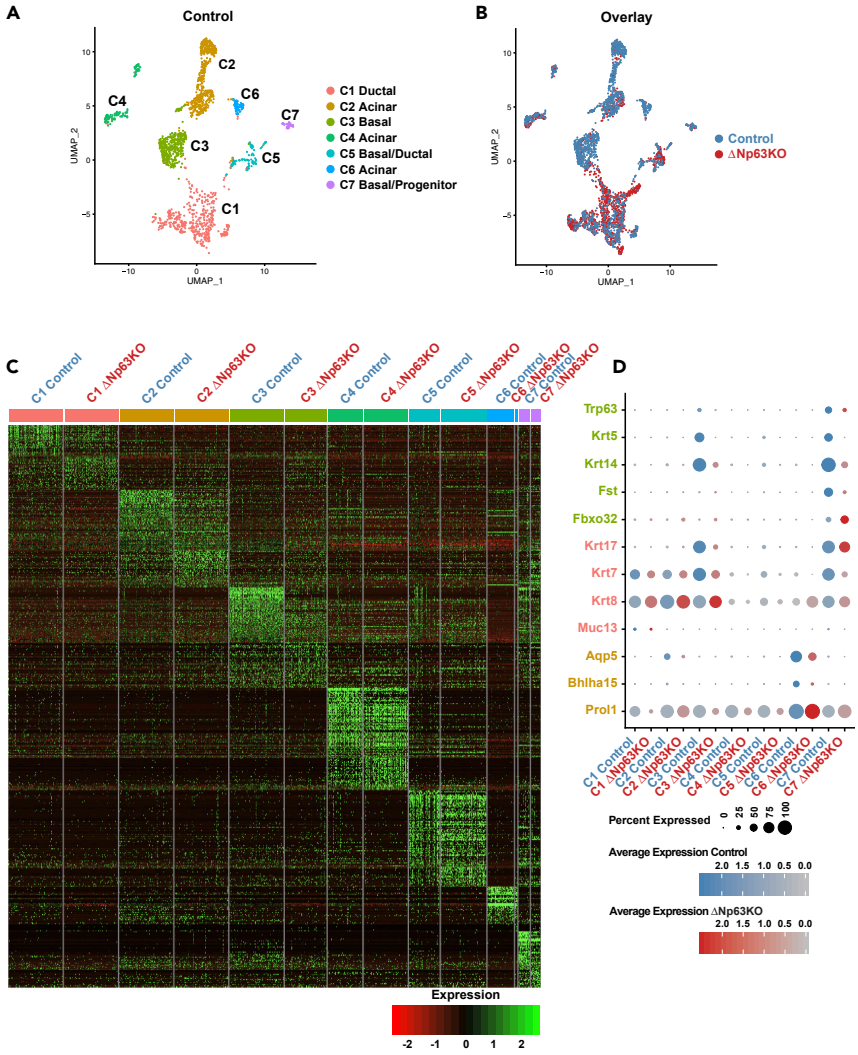

Figure 4. Single-Cell RNA Sequencing Analysis Reveals ΔNp63-Dependent Cellular States

(A) UMAP visualization of the various epithelial cell populations in control adult mouse SMG.

(B) UMAP projection overlays of epithelial cell populations from the control and ΔNp63KO adult SMG.

(C) Heatmap depicts the top 100 differentially expressed genes in each cluster as compared with all clusters between control and KO SMGs. Upper bars represent cluster assignments.

(D) Dot plot of proportion of cells in each cluster expressing each marker (dot size), and average expression (color scale) of known basal (*Trp63*, *Krt5*, *Krt14* and *Fst*), ductal (*Krt17*, *Krt7*, *Krt8*, *Muc13*), and acinar (*Aqp5*, *Bhlha15*, *Prol1*) genes in control mice compared with KO. C, cluster; UMAP, uniform manifold approximation and projection.

See also Figure S5 and Tables S2 and S3.

Single-Cell Analysis Reveals the Requirement of ΔNp63 in Maintaining the Stem/Progenitor Cell Population in the Salivary Gland

To obtain a more detailed understanding of the cellular states and further interrogate the role of ΔNp63 in the adult SG at single-cell resolution, we performed scRNA-seq analysis of control and ΔNp63KO adult SMGs. We first established the global structure of the dataset by performing unsupervised clustering with affinity propagation based on the expression of high variance genes in the control animals (Frey and Dueck, 2007). This analysis identified seven distinct groups of epithelial cells, which we visualized via uniform manifold approximation and projection (UMAP) (Figure 4A). Cell type assignments were made based on the expression of known/validated marker genes similar to what we and others have previously reported in both the SMG and PG (Table S2) (Song et al., 2018; Oyelakin et al., 2019; Sekiguchi et al., 2020). Integrated analysis of control and ΔNp63KO datasets revealed striking differences between the various cell

populations (Figure 4B). For example, compared with the control cells, ΔNp63KO cells revealed reduced numbers of cells that comprised the acinar clusters (C2 and C6) (Figure 4B). Although this finding was surprising given that ΔNp63 expression was not detected in the acinar cells, it does correlate well with the reduced Amy1 protein expression levels we observed in our immunofluorescence analysis, confirming alterations to this cell lineage in the absence of ΔNp63 (Figures 1F and S1B). Conversely, in the KO glands we observed increased numbers of cells in cluster C1, representing ductal cells, and cluster C5, which represent mixed basal and ductal cell lineages (Figure 4B). These differences are further highlighted in Figure 4C in which the top 100 DEGs across all clusters between the control and KO glands are shown (Figure 4C and Table S3). A subset of DEGs are shown in Figure 4D. Our analysis also revealed reduced numbers of basal cells represented in C3 and C7 in the ΔNp63KO glands, which is in good agreement with previous studies demonstrating a role for p63 in directing basal specific keratin gene expression and in directing epidermal cell fate specification in the skin (Figures 4B and 4D) (Romano et al., 2009; Fan et al., 2018).

In order to probe further into the ΔNp63-driven mechanisms underlying the cellular changes in the SG, we focused on cluster 7 of the control mice for further analysis. We reasoned that, since this cell population demonstrated the highest expression levels of *Trp63* mRNA as compared with C3, it likely represented the SP cell population (Figure 4D). This notion is based on previous studies that have shown that p63 expression is highest in epithelial cells with high clonogenic potential, whereas low levels of p63 expression is associated with reduced proliferative capacity (Senoo et al., 2007; Pellegrini et al., 2001). With this in mind, we mined our scRNA-seq dataset and performed Gene Ontology (GO) analysis using the genes enriched in cluster C7 of the control glands (Figures 4A and Table S2). Indeed, our analysis identified overrepresentation of genes associated with biological pathways that included negative regulation of epithelial cell differentiation, gland morphogenesis, and regulation of epithelial cell proliferation (Figure S5). We also observed specific enrichment in somatic stem cell population maintenance and tissue regeneration, pointing to the possibility that this cluster may represent an SP cell population (Figure S5). Having identified negative regulation of cellular response to TGF-β stimulus as one of the top enriched biological pathways, we decided to focus our attention on the TGF-β signaling pathway. This was spurred by previous reports demonstrating that inhibition of TGF-β signaling leads to increased proliferative capacity of $p63^{+ve}$ epidermal progenitor cells (Mou et al., 2016; Suzuki et al., 2017). Interestingly, further mining of the bulk RNA-seq datasets revealed elevated mRNA expression levels of a number of genes involved in TGF-β signaling in the ΔNp63KO mice, suggesting that the loss of ΔNp63 expression results in activation of this signaling pathway (Figure S6). A possible explanation that may account for the aberrant activation of TGF-β signaling in the KO mice may be due to altered expression levels of several molecular players important in Activin signaling including activin receptors *Acrv1* and *Acrv1b* as well as Activin downstream effectors *Smad2* and *Smad3* (Figure S6). Follistatin (Fst) is a soluble extracellular protein that acts as a key inhibitor of Activin signaling. Fst exerts its function by binding to circulating activin and preventing it from binding to its receptor and activating a downstream signaling cascade that results in phosphorylation and activation of Smad2/3. Indeed, we identified *Fst* as one of the top downregulated genes in the KO glands, similar to what we have previously reported in the skin epidermis of ΔNp63KO mice (Figure S6) (Fan et al., 2018). Although Fst has been shown to play key roles in skin and tooth morphogenesis and in maintaining thymic epithelial progenitor cells in an undifferentiated state, its role in the SMG has not been investigated (Lepletier et al., 2019; Matzuk et al., 1995; Nakamura et al., 2003).

ΔNp63 Mediates Salivary Gland Stem/Progenitor Cell Function by Directly Regulating Follistatin Expression

The dramatic downregulation of *Fst* mRNA gene expression evident from bulk RNA-seq and scRNA-seq data (Figures S6 and 4D), and confirmed by qRT-PCR (Figure 2E), prompted us to examine the *in vivo* expression profile of ΔNp63 and Fst in the SG and to test if *Fst* might be a direct transcriptional target of ΔNp63. Toward this end, we first sought to determine whether these two factors were co-expressed in the SMG, by performing RNAscope analysis. As expected, we found *Trp63* and *Fst* mRNA to be co-expressed in the basal cells of the adult mouse SMG, similar to what has been reported in the murine skin epidermis (Figure S7) (Nakamura et al., 2003). This was further supported by our scRNA-seq studies, which revealed specific enrichment of *Trp63* and *Fst* in cluster C7 (Figure 4D). Having established the co-localization of *Trp63* and *Fst*, we next performed ChIP-seq experiments in pSEPCs with anti-p63 and anti-H3K27Ac antibodies to identify global ΔNp63-binding events and enhancers, respectively. Our ChIP-seq studies identified a large cohort of ~4,000 ΔNp63 target genes and importantly revealed a ΔNp63-binding region downstream of the *Fst* genomic locus, suggesting that *Fst* is a direct transcriptional target of ΔNp63 (Figure 5A). Moreover, the ΔNp63-bound regulatory region represented

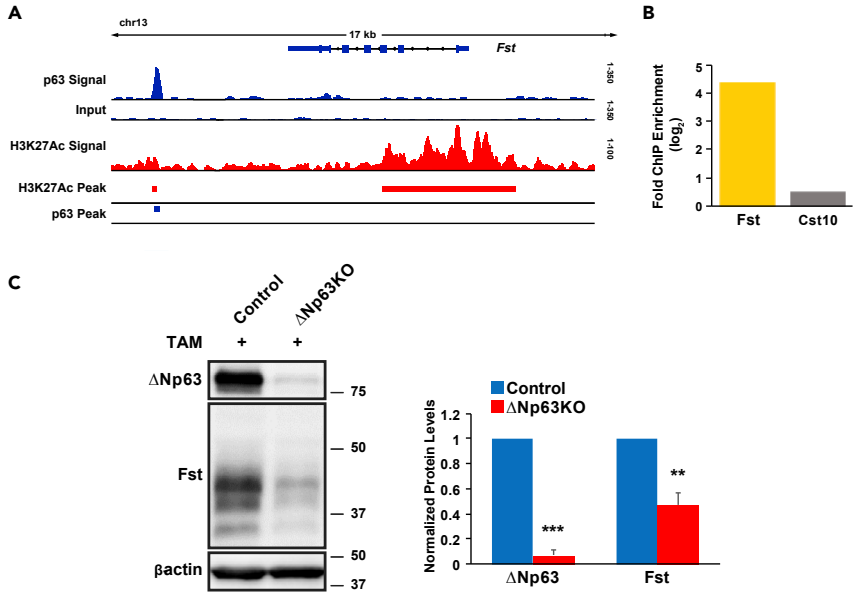

Figure 5. Direct Regulation of *Fst* Expression by ΔNp63

(A) Visualization of ΔNp63 interaction with the target gene *Fst* (Integrated Genomics Viewer). Top two lines display p63 ChIP signal enrichment, relative to Input, located at an enhancer near the *Fst* gene locus in pSEPCs. Third line displays H3K27Ac ChIP signal around the *Fst* genomic locus. Bottom two lines depict the p63 binding site (black box) and active enhancers (red boxes) within the pSEPCs.

(B) Independent ChIP qPCR results using a ΔNp63 antibody in pSEPCs confirms specific binding of p63 to the *Fst* genomic locus. *Cst* serves as a negative control. Values represent mean fold enrichment over the random genomic locus (*Cst*).

(C) Representative western blot analysis of control and ΔNp63KO pSEPCs treated with TAM reveals robust knockdown of ΔNp63 and Fst protein expression levels in the KO cells compared with control. ΔNp63 and Fst protein expression were normalized to β-actin. Quantification is shown on the right. Data are represented as mean ± SD (n = 3). **p < 0.01, ***p < 0.001.

See also Figure S7.

an active enhancer site as demonstrated by enriched H3K27Ac peaks (Figure 5A). To confirm our ChIP-seq results, we performed an independent ChIP on mouse pSEPCs followed by quantitative-polymerase chain reaction (qPCR) quantification. To ensure the validity and specificity of our ChIP studies, we included an intragenic region within the *Cst10* gene, which does not contain a p63 response element, to serve as a negative control. Indeed, our qPCR results demonstrated selective enrichment of the putative p63 response element in the *Fst* genomic locus relative to the control region (Figure 5B). Next, to test the functional consequences of p63 binding to this potential regulatory element we performed p63 knockdown (KD) experiments. Primary salivary gland epithelial cells isolated from control and ΔNp63KO mice were treated with activated TAM to specifically KD ΔNp63 expression. Indeed, western blot analysis revealed reduced protein expression levels of ΔNp63 and Fst in the ΔNp63KO cells as compared with control cells (Figure 5C). Taken together, these data strongly suggest that ΔNp63 can directly regulate the expression of Fst, which may account for the aberrant activation of Activin signaling leading to reduced proliferative potential of SG SP cells upon the loss of p63 expression.

Prior studies have demonstrated a role for Fst in maintaining thymic epithelial progenitor cells in an immature state (Lepletier et al., 2019). To test if Fst functions similarly in the SP cells of the SG we performed clonogenic assays in primary pSEPCs treated with increasing concentrations of Fst. Interestingly, addition of Fst resulted in increased clonogenic potential compared with control non-Fst treated cells (Figure S8). Having established a role for Fst in maintaining clonogenicity in pSEPCs, we next wondered if the addition of Fst could rescue the reduced clonogenic properties observed upon the loss of ΔNp63. To address this, we performed clonogenic assays on pSEPCs isolated from ΔNp63KO mice that were treated with TAM in the presence or absence of Fst. Indeed, compared with TAM-treated cells alone, pSEPCs treated with both TAM and Fst resulted in increased clonogenic capabilities suggesting that Fst is able to compensate for the loss of ΔNp63 expression and maintain the proliferative potential of SG SP cells (Figure 6A).

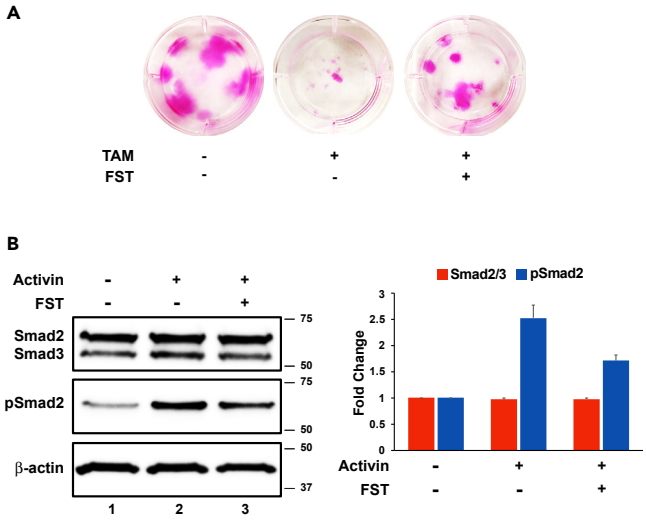

Figure 6. Fst is a Key Modulator of Activin Signaling in Salivary Gland Epithelial Progenitor Cells

(A) Representative images of Rhodamine B staining of ΔNp63KO pSEPCs clones treated with TAM to KD ΔNp63 expression in the absence or presence of Fst. Clones were grown for 14 days. Fst is able to rescue the clonogenic defects observed upon the loss of ΔNp63 expression.

(B) Western blot showing the effects of Fst on Activin signaling in pSEPCs. Treatment with Activin A results in Smad2 phosphorylation, whereas addition of Fst attenuates phosphorylation (compare lanes 2 and 3). Smad 2, Smad 3, and pSmad2 protein expression levels were normalized to β-actin. A quantification is shown on the right.

Data are represented as mean ± SD (n = 3) *p < 0.05. See also Figures S8 and S9.

The Fst/Activin/Smad Signaling Axis Maintains the Clonogenic Potential of Salivary Gland Stem/Progenitor Cells

Having established the effects of Fst on the clonogenic properties of the SP cells in the SG, we next sought to investigate the mechanism through which Fst exerts its downstream effects. We first investigated the phosphorylation state of the various Smad proteins as a readout of BMP and activin signaling in the pSEPCs. Interestingly, western blot analysis of p-Smad1/5/8 revealed that BMP signaling was not active in these cells under normal growth conditions (Figure S9A). However, when pSEPCs were treated with increasing concentrations of BMP, increased Smad1/5/8 phosphorylation was observed (Figure S9A). In contrast, Activin signaling was constitutively active since we observed robust expression of pSmad2, which increased when pSEPCs were treated with increasing concentrations of Activin A (Figure S9B). In contrast, we did not detect expression of pSmad3. In light of these results, we focused our attention on Activin signaling. In order to assess the functional impact of Fst on Activin signaling, we treated pSEPCs with Activin A, which activated the pathway as demonstrated by increased pSmad2 expression levels as compared with untreated cells (Figure 6B left panel, compare lane 1 and lane 2). We next treated the cells with Activin A in the presence of Fst and determined the effects of Fst on Activin signaling. Indeed, the addition of Fst resulted in the attenuation of Activin A signaling as shown by reduced pSmad2 protein expression levels (Figure 6B left panel, compare lane 2 and lane 3). Overall, these data suggest a role for Fst in driving the clonogenic potential of SG SP cells by modulating Activin A signaling.

DISCUSSION

ΔNp63 is highly enriched in the stem/progenitor cell populations of epithelial-rich tissues including the SG, where it plays indispensable roles in maintaining proliferative potential as well as directing lineage commitment and cell fate choices (Blanpain and Fuchs, 2007; Senoo et al., 2007). Although previous work has focused on epithelial tissues including those of the skin, mammary gland, and prostate, mechanistic studies on the SMG have been lacking. Here we have provided a comprehensive analysis of the effects of ablation of the transcription factor ΔNp63 in the SMG of adult mice. We find that loss of ΔNp63 expression in the basal/myoepithelial cells of adult mice resulted in wide-ranging effects including altered ductal and acinar cell differentiation and impaired SP cell function leading to the eventual loss of this important cell population.

One surprising yet interesting observation was the broad differentiation defects in the SG due to ΔNp63 loss such as those of the acinar and ductal cells, which do not express ΔNp63. These far-reaching effects of ΔNp63 fit well with results from our recent genetic lineage tracing experiments, which demonstrated that ΔNp63^{+ve} basal cells serve as predecessor stem cells to several different cellular subpopulations. Remarkably, the cell fate transition process of ΔNp63^{+ve} basal cells under homeostatic conditions is relatively rapid as the ΔNp63-derived cells are detected in the ductal luminal cells of the SMG in as little as 1 week (Song et al., 2018). Our findings are in line with genetic lineage tracing experiments performed in salivary glands of adult mice showing that the transition of actively proliferating K14^{+} basal cells to both the ductal intercalated and excretory luminal cells of the gland occurs fairly quickly—within 14 days (Kwak et al., 2016; Kwak and Ghazizadeh, 2015). Moreover, the wide-spread defects observed upon the loss of ΔNp63 in the SG are also in good agreement with similar studies reported in the mammary gland (Forster et al., 2014; Kumar et al., 2019). Interestingly, conditional deletion of ΔNp63 in the pubertal mammary gland results in aberrant ductal formation presumably owing to altered stem cell differentiation (Kumar et al., 2019). Moreover, ΔNp63 has also been shown to be important during pregnancy as ΔNp63KO mice showed defects in luminal progenitor cell proliferation and differentiation (Forster et al., 2014). These animals displayed a complete block in the development of milk-producing alveolar cells, which are functionally similar to the saliva-secreting acinar cells of the SG. The mechanism through which p63 directs luminal progenitor cell differentiation and alveologenesis in the mammary gland involves paracrine signaling and activation of the Nrg1/Erbb4/Stat5a signaling axis, whereas this is unlikely to be the case in the SG as components of this signaling pathway are not expressed in this organ (Table S1). The physiological defects that stem from maturation deficiency of the alveolar cells of the mammary gland and the acinar cells of the SG suggests that ΔNp63 may play a broader and pervasive role in modulating the secretory cell outputs of glandular tissues. Given the importance of acinar cells and the effects of loss of salivary secretion in diseases such as Sjögren's syndrome or due to off-target effects of γ-irradiation therapy in patients with oral cancers, identifying the molecular mechanisms through which p63 acts on this cell population warrants further investigation.

Although our analysis has revealed a number of significant alterations to acinar and ductal cell differentiation, one of the most striking observations were the dramatic effects to the SP cells, which included not only reduced proliferative and clonogenic potentials but also a distinct loss of this important cell population. Although these results are in good agreement with similar observations that have been reported in the thymus, skin, and mammary gland, where p63 has been shown to maintain stem cell "stemness," the underlying molecular mechanisms through which ΔNp63 maintains the proliferative and self-renewal states of this cell type has been lacking. Recent studies have suggested a link between p63 and the TGF-β superfamily signaling pathway in maintaining the proliferative potential of epithelial progenitor cells. Indeed, Mou et al. have shown that TGF-β/BMP/SMAD signaling is activated specifically in the luminal and suprabasal cells of stratified epithelium where it promotes cellular differentiation while being suppressed in the basal cells where p63 is highly expressed (Mou et al., 2016). This notion is further supported by *in vitro* studies demonstrating that inhibition of TGF-β signaling results in the increased proliferative potential of diverse epithelial progenitor cells (Suzuki et al., 2017). Interestingly, TGF-β inhibition results in the enrichment and expansion of p63^{+ve} progenitor cells. Although these studies collectively support the possibility of p63 functioning as an upstream regulator of the TGF-β signaling axis in maintaining stem progenitor cell immature states, the molecular mechanism through which p63 and TGF-β coordinate to direct these processes has not been elucidated (Mou et al., 2016; Suzuki et al., 2017). Based on our integrated analysis of transcriptomic (RNA-seq, scRNA-seq) and genomic (ΔNp63 ChIP-seq) studies we have identified Follistatin (Fst) as a putative candidate in maintaining the clonogenic potential of pSEPCs by inhibiting Activin signaling, similar to what has been reported in thymic epithelial progenitor cells (Lepletier et al., 2019). Moreover, our data demonstrate that Fst can rescue the clonogenic defects associated with the loss of ΔNp63 suggesting an intrinsic link between p63 and Fst in directing differentiation programs in SP cells. Taken together, our studies have identified Fst as an important molecular link in the genetic circuitry through which p63 coordinates with the Activin/Smad signaling pathway in maintaining the proliferative potential of pSEPCs (Figure 7). We posit that the intimate regulatory circuitry between Fst/Activin/p63 that underlies stem cell specification as described here might also be in play in other tissues and organs as evident by a recent report of this signaling axis as a mediator of telomere dysfunction in the mouse skin epidermis (Liu et al., 2019). Long term, unearthing the molecular mechanisms regulating the differentiation and self-renewal programs of SP cells has important implications for both regenerative medicine and understanding how these programs contribute to tumorigenesis.

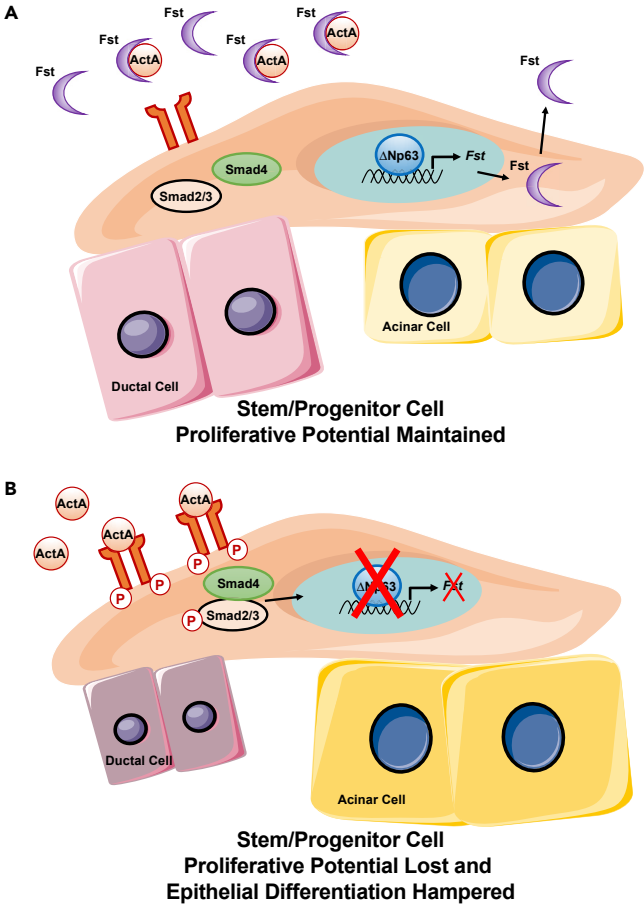

Figure 7. ΔNp63^{+ve} Basal/Myoepithelial Cells Maintain the Proliferative Potential of Salivary Gland Epithelial Progenitor Cells Through Activation of the Follistatin/Activin/Smad Signaling Axis

(A) p63 directly regulates the expression of *Fst*, which functions as a potent antagonist of Activin signaling. Fst maintains the proliferative potential of pSEPCs by sequestering Activin A and preventing it from binding to its receptor and acting on its downstream effectors, phosphorylated Smad2/3.

(B) Ablation of p63 results in the loss of Fst expression and activation of Activin signaling resulting in the loss of salivary gland stem/progenitor cell proliferative potential. This is accompanied by alterations in ductal and acinar cell differentiation resulting in reduced ductal cell size and enlarged acinar cells, respectively.

Limitations of the Study

In the present study, we have leveraged genetic models and genomic interrogation techniques to uncover a critical role for p63 as a regulator of the Follistatin/Activin/Smad signaling axis to maintain stem/progenitor cell function. Our *in vitro* studies have focused on the role of p63 in the epithelial stem/progenitor cells in regulating Activin/Smad signaling; a limitation to this model system is that it does not examine the possibility of cross talk between the epithelium and the mesenchyme, in this process. Additionally, the inherent limitations associated with scRNA sequencing coupled with the lack of reliable markers have limited our ability to identify the various cellular populations that comprise the SMG.

Resource Availability

Lead Contact

Further information and requests for resources and reagents should be directed to and will be fulfilled by the Lead Contact, Rose-Anne Romano (rromano2@buffalo.edu).

Materials Availability

This study did not generate new materials.

Data and Code Availability

Bulk RNA-seq, ChIP-seq, and scRNA-seq files have been uploaded to the Gene Expression Omnibus (GSE accession number GSE145268).

METHODS

All methods can be found in the accompanying Transparent Methods supplemental file.

SUPPLEMENTAL INFORMATION

Supplemental Information can be found online at https://doi.org/10.1016/j.isci.2020.101524.

ACKNOWLEDGMENTS

This work was supported by National Institutes of Health/National Institute of Dental and Craniofacial Research (NIH/NIDCR) grants DE025889 and DE027660 to R.-A.R. A.O., E.-A.C.S., and S.M. were supported by the State University of New York at Buffalo, School of Dental Medicine, Department of Oral Biology training grant (NIH/NIDCR) DE023526.

AUTHOR CONTRIBUTIONS

S.M., S.S., and R.-A.R. designed the experiments. S.M., A.O., E.-A.C.S., K.S., and R.-A.R. performed experiments. E.F. provided essential tools. S.M., C.G., A.O., J.E.B., E.-A.C.S., K.S., M.C., and R.-A.R. analyzed the data. S.M., S.S., and R.-A.R. wrote the paper. All authors reviewed and edited the drafts and approved the final version.

DECLARATION OF INTERESTS

The authors declare no competing interests.

Received: May 14, 2020
Revised: July 13, 2020
Accepted: August 28, 2020
Published: September 25, 2020

REFERENCES

Amano, O., Mizobe, K., Bando, Y., and Sakiyama, K. (2012). Anatomy and histology of rodent and human major salivary glands: overview of the Japan salivary gland society-sponsored workshop. Acta Histochem. Cytochem. *45*, 241–250.

Blanpain, C., and Fuchs, E. (2007). p63: revving up epithelial stem-cell potential. Nat. Cell Biol. *9*, 731–733.

Chakrabarti, R., Wei, Y., Hwang, J., Hang, X., Andres Blanco, M., Choudhury, A., Tiede, B., Romano, R.A., Decoste, C., Mercatali, L., et al. (2014). DeltaNp63 promotes stem cell activity in mammary gland development and basal-like breast cancer by enhancing Fzd7 expression and Wnt signalling. Nat. Cell Biol. *16*, 1004–1015.

Chakravarti, D., Su, X., Cho, M.S., Bui, N.H., Coarfa, C., Venkatanarayan, A., Benham, A.L., Flores Gonzalez, R.E., Alana, J., Xiao, W., et al. (2014). Induced multipotency in adult keratinocytes through down-regulation of DeltaNp63 or DGCR8. Proc. Natl. Acad. Sci. U S A *111*, E572–E581.

Fan, X., Wang, D., Burgmaier, J.E., Teng, Y., Romano, R.A., Sinha, S., and Yi, R. (2018). Single cell and open chromatin analysis reveals molecular origin of epidermal cells of the skin. Dev. Cell *47*, 21–37 e5.

Forster, N., Saladi, S.V., Van Bragt, M., Sfondouris, M.E., Jones, F.E., Li, Z., and Ellisen, L.W. (2014). Basal cell signaling by p63 controls luminal progenitor function and lactation via NRG1. Dev. Cell *28*, 147–160.

Frey, B.J., and Dueck, D. (2007). Clustering by passing messages between data points. Science *315*, 972–976.

Harunaga, J., Hsu, J.C., and Yamada, K.M. (2011). Dynamics of salivary gland morphogenesis. J. Dent. Res. *90*, 1070–1077.

Kumar, S., Nandi, A., Mahesh, A., Sinha, S., Flores, E., and Chakrabarti, R. (2019). Inducible knockout of Np63 alters cell polarity and metabolism during pubertal mammary gland development. FEBS Lett. *594*, 973–985.

Kwak, M., Alston, N., and Ghazizadeh, S. (2016). Identification of stem cells in the secretory complex of salivary glands. J. Dent. Res. *95*, 776–783.

Kwak, M., and Ghazizadeh, S. (2015). Analysis of histone H2BGFP retention in mouse submandibular gland reveals actively dividing stem cell populations. Stem Cells Dev *24*, 565–574.

Lee, D.K., Liu, Y., Liao, L., Wang, F., and Xu, J. (2014). The prostate basal cell (BC) heterogeneity and the p63-positive BC differentiation spectrum in mice. Int. J. Biol. Sci. *10*, 1007–1017.

Lepletier, A., Hun, M.L., Hammett, M.V., Wong, K., Naeem, H., Hedger, M., Loveland, K., and Chidgey, A.P. (2019). Interplay between follistatin, activin A, and BMP4 signaling regulates postnatal thymic epithelial progenitor cell differentiation during aging. Cell Rep. *27*, 3887–3901.e4.

Liu, N., Yin, Y., Wang, H., Zhou, Z., Sheng, X., Fu, H., Guo, R., Wang, H., Yang, J., Gong, P., et al. (2019). Telomere dysfunction impairs epidermal stem cell specification and differentiation by disrupting BMP/pSmad/P63 signaling. PLoS Genet. *15*, e1008368.

Massague, J. (2012). TGFbeta signalling in context. Nat. Rev. Mol. Cell Biol. *13*, 616–630.

Matzuk, M.M., Lu, N., Vogel, H., Sellheyer, K., Roop, D.R., and Bradley, A. (1995). Multiple defects and perinatal death in mice deficient in follistatin. Nature *374*, 360–363.

Mou, H., Vinarsky, V., Tata, P.R., Brazauskas, K., Choi, S.H., Crooke, A.K., Zhang, B., Solomon, G.M., Turner, B., Bihler, H., et al. (2016). Dual SMAD signaling inhibition enables long-term

expansion of diverse epithelial basal cells. Cell Stem Cell *19*, 217–231.

Nakamura, M., Matzuk, M.M., Gerstmayer, B., Bosio, A., Lauster, R., Miyachi, Y., Werner, S., and Paus, R. (2003). Control of pelage hair follicle development and cycling by complex interactions between follistatin and activin. FASEB J. *17*, 497–499.

Nanduri, L.S., Baanstra, M., Faber, H., Rocchi, C., Zwart, E., De Haan, G., Van Os, R., and Coppes, R.P. (2014). Purification and ex vivo expansion of fully functional salivary gland stem cells. Stem Cell Rep. *3*, 957–964.

Nanduri, L.S., Maimets, M., Pringle, S.A., Van Der Zwaag, M., Van Os, R.P., and Coppes, R.P. (2011). Regeneration of irradiated salivary glands with stem cell marker expressing cells. Radiother. Oncol. *99*, 367–372.

Oshimori, N., and Fuchs, E. (2012). The harmonies played by TGF-beta in stem cell biology. Cell Stem Cell *11*, 751–764.

Oyelakin, A., Song, E.A.C., Min, S., Bard, J.E., Kann, J.V., Horeth, E., Smalley, K., Kramer, J.M., Sinha, S., and Romano, R.A. (2019). Transcriptomic and single-cell analysis of the murine parotid gland. J. Dent. Res. *98*, 1539–1547.

Packard, A., Schnittke, N., Romano, R.A., Sinha, S., and Schwob, J.E. (2011). DeltaNp63 regulates stem cell dynamics in the mammalian olfactory epithelium. J. Neurosci. *31*, 8748–8759.

Pellegrini, G., Dellambra, E., Golisano, O., Martinelli, E., Fantozzi, I., Bondanza, S., Ponzin, D., Mckeon, F., and De Luca, M. (2001). p63 identifies keratinocyte stem cells. Proc. Natl. Acad. Sci. U S A *98*, 3156–3161.

Pringle, S., Maimets, M., Van Der Zwaag, M., Stokman, M.A., Van Gosliga, D., Zwart, E., Witjes, M.J., De Haan, G., Van Os, R., and Coppes, R.P. (2016). Human salivary gland stem cells functionally restore radiation damaged salivary glands. Stem Cells *34*, 640–652.

Pringle, S., Van Os, R., and Coppes, R.P. (2013). Concise review: adult salivary gland stem cells and a potential therapy for xerostomia. Stem Cells *31*, 613–619.

Romano, R.A., Ortt, K., Birkaya, B., Smalley, K., and Sinha, S. (2009). An active role of the DeltaN isoform of p63 in regulating basal keratin genes K5 and K14 and directing epidermal cell fate. PLoS One *4*, e5623.

Romano, R.A., Smalley, K., Magraw, C., Serna, V.A., Kurita, T., Raghavan, S., and Sinha, S. (2012). {Delta}Np63 knockout mice reveal its indispensable role as a master regulator of epithelial development and differentiation. Development *139*, 772–782.

Sekiguchi, R., Martin, D.; Genomics, Computational Biology, Core, and Yamada, K.M. (2020). Single-cell RNA-seq identifies cell diversity in embryonic salivary glands. J. Dent. Res. *99*, 69–78.

Senoo, M., Pinto, F., Crum, C.P., and McKeon, F. (2007). p63 Is essential for the proliferative potential of stem cells in stratified epithelia. Cell *129*, 523–536.

Song, E.C., Min, s., Oyelakin, a., Smalley, K., Bard, J.E., Liao, L., Xu, J., and Romano, R.A. (2018). Genetic and scRNA-seq analysis reveals distinct cell populations that contribute to salivary gland development and maintenance. Sci. Rep. *8*, 14043.

Suzuki, d., Pinto, f., and Senoo, M. (2017). Inhibition of TGF-beta signaling supports high proliferative potential of diverse p63(+) mouse epithelial progenitor cells in vitro. Sci. Rep. *7*, 6089.

Tucker, A.S. (2007). Salivary gland development. Semin. Cell Dev. Biol. *18*, 237–244.

Wu, M.Y., and Hill, C.S. (2009). Tgf-beta superfamily signaling in embryonic development and homeostasis. Dev. Cell *16*, 329–343.

iScience, Volume *23*

Supplemental Information

p63 and Its Target Follistatin Maintain Salivary Gland Stem/Progenitor Cell Function through TGF-β/Activin Signaling

Sangwon Min, Akinsola Oyelakin, Christian Gluck, Jonathan E. Bard, Eun-Ah Christine Song, Kirsten Smalley, Monika Che, Elsa Flores, Satrajit Sinha, and Rose-Anne Romano

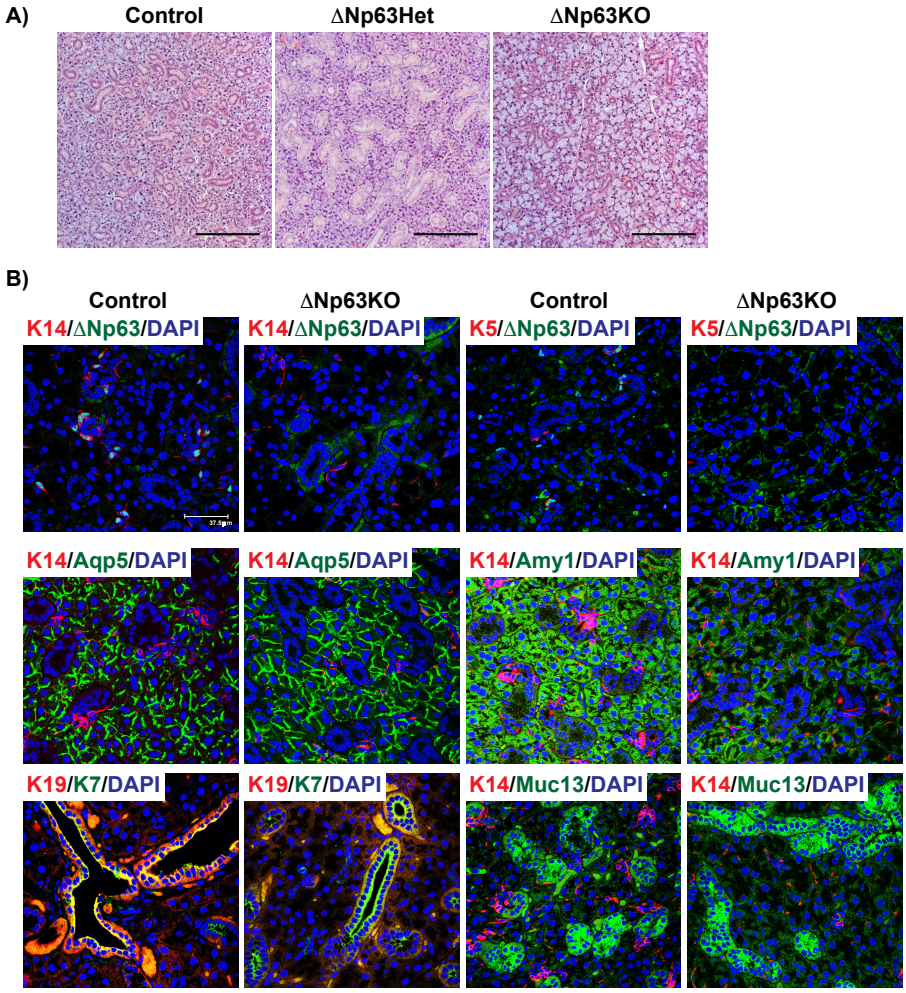

Figure S1. Histological and Immunochemical Analysis of Submandibular Salivary Glands of Female Mice with Targeted Deletion of ΔNp63. Related to Figure 1. (A) H&E staining of control, ΔNp63Het and ΔNp63KO female SMGs. Compared to control and ΔNp63Het glands, KO mice show reduced ductal size along with enlarged acini. Scale bar: 200μm. (B) Immunofluorescence staining of control and ΔNp63KO glands confirm the loss of ΔNp63 expression as well as a dramatic reduction in the K5 and K14 stem/progenitor cell population. Alterations to the acinar cell differentiation program is also observed in the KO glands as evident by the loss of Amy1 expression. While K7 and Muc13 expression levels appear unchanged in the

ducts of the KO glands, K19 expression is reduced compared to control glands. Scale bar: 37.5μm.

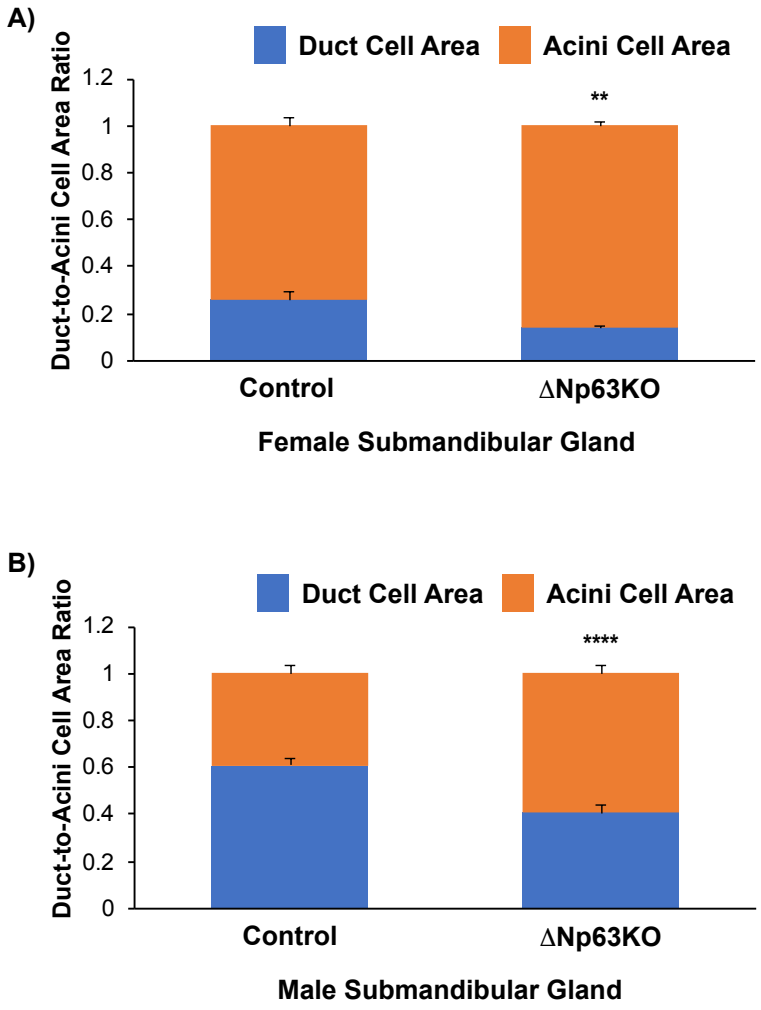

Figure S2. Quantification of Duct-to-Acini Cell Area Ratio in Submandibular Salivary Glands of Female and Mice with Targeted Deletion of ΔNp63. Related to Figure 1. Quantification analysis of the ratio of duct cell area compared to acini cell area in female (A) and male (B) control and ΔNp63KO SMG as indicated. Data are represented as ± S.D (n=4) $^{**}p<0.01$, $^{****}p<0.0001$.

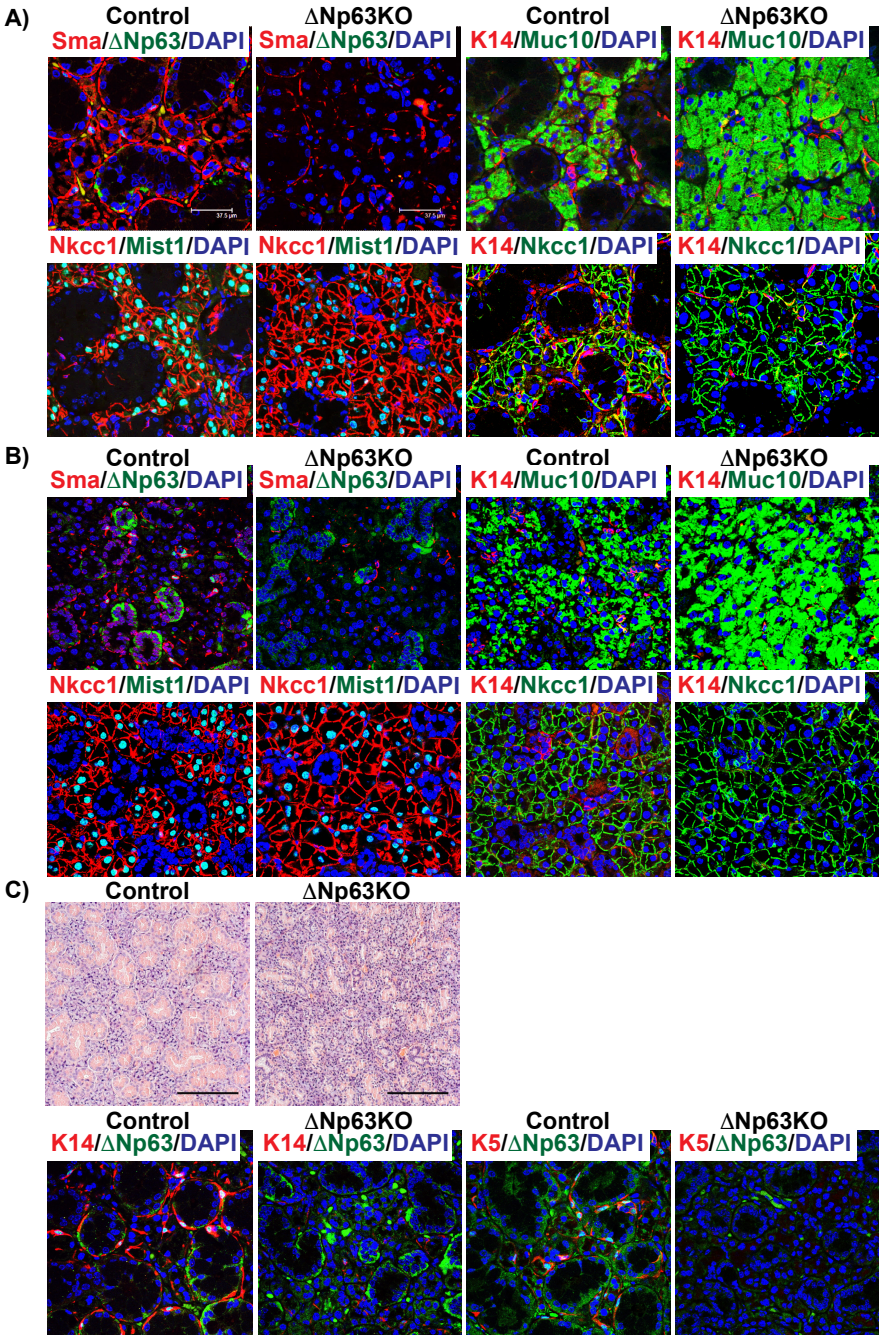

Figure S3. Immunochemical Analysis of ΔNp63KO Submandibular Salivary Glands. Related to Figure 1. (A) Immunofluorescence staining analysis of a panel of various differentiation markers on SMGs harvested from adult control and ΔNp63KO male and female (B) glands. (C) Histological and immunochemical staining of male *Trp63*^{CreERT2}*;ΔNp63*$^{fl/fl}$ SMGs

demonstrates a similar phenotype to that of the *UBC*^{CreERT2}*;*Δ*Np63*$^{fl/fl}$ mice. Upper panel scale bar: 200μm, lower panel scale bar: 37.5μm.

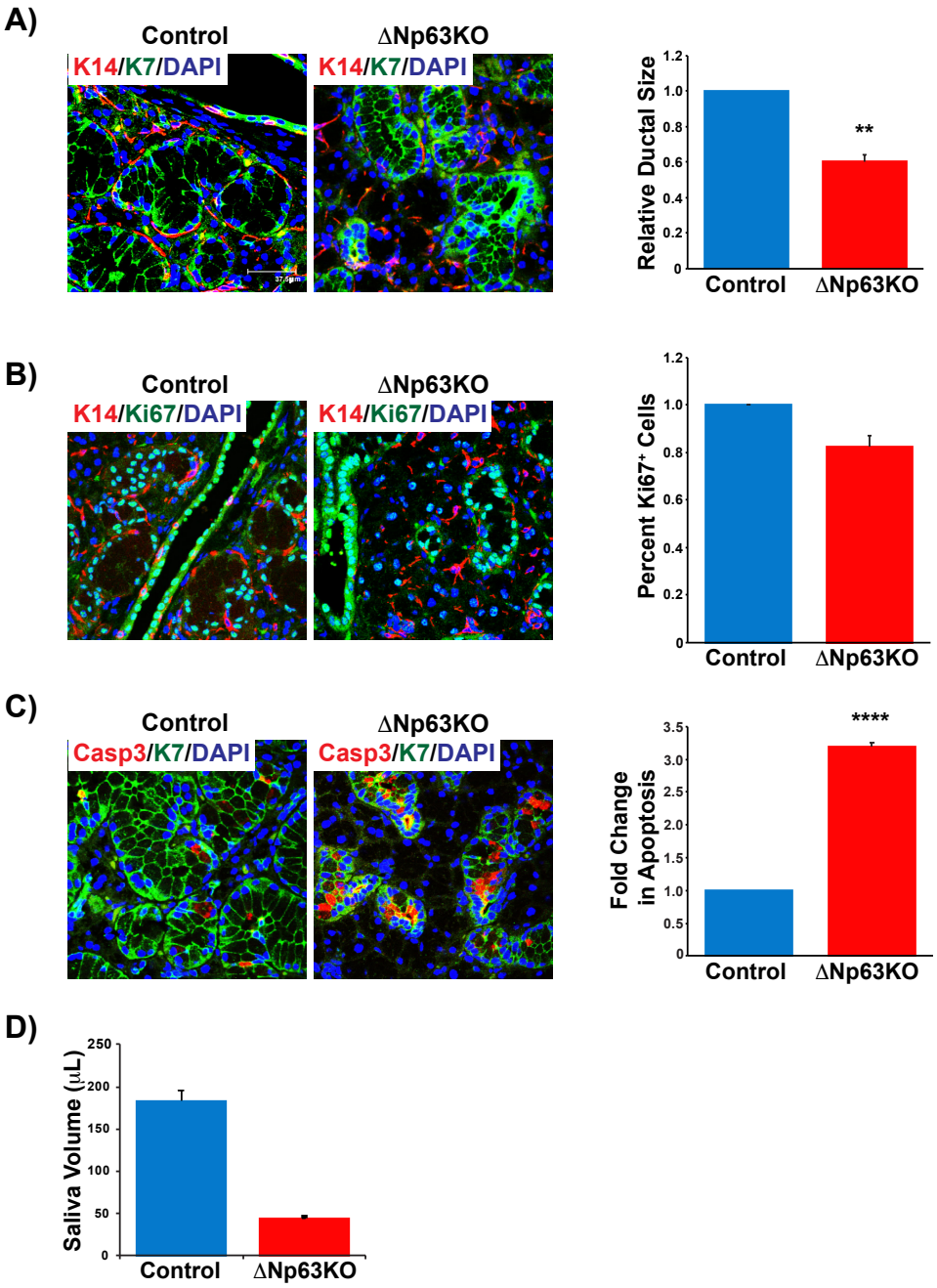

Figure S4. Ductal Cells Undergo Apoptosis in the Absence of ΔNp63. Related to Figure 1.

(A) Expression and quantification analysis of ducts stained with K7 shows a reduction in the overall size of the ducts as well as smaller ductal cells in the KO glands. (B) Expression and quantification analysis of cell proliferation using the proliferation marker Ki67, shows a modest reduction in the KO as compared to the control glands. (C) Expression and quantification analysis

of cleaved caspase-3 reveals increased ductal cell apoptosis in the KO. (D) Saliva production was quantified from control and KO mice. Data are represented as ± S.D (n=3) $^{**}p<0.01$, $^{****}p<0.0001$. Scale bar: 37.5μm.

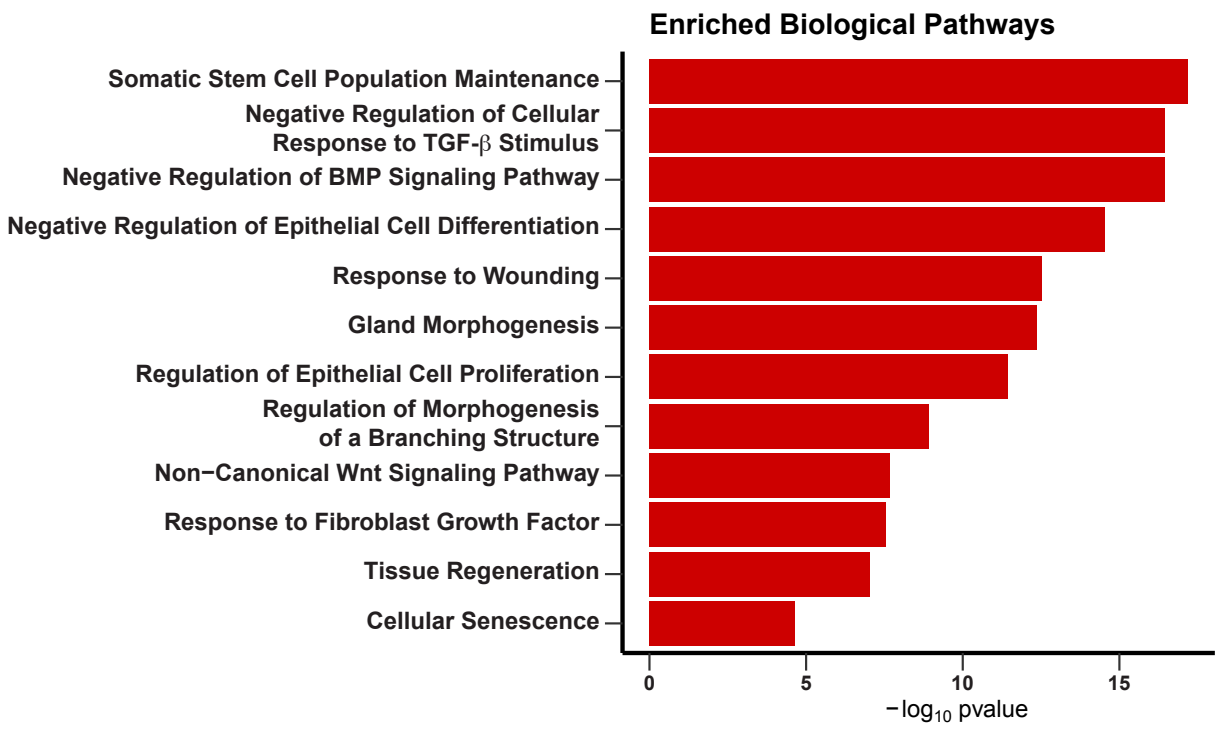

Figure S5. Enriched Biological Process Networks in the Putative Stem/progenitor Cell Cluster 7. Related to Figure 4. Bar plot highlights the top enriched biological processes in control SMGs as identified by scRNA-seq analysis (Figure 4A).

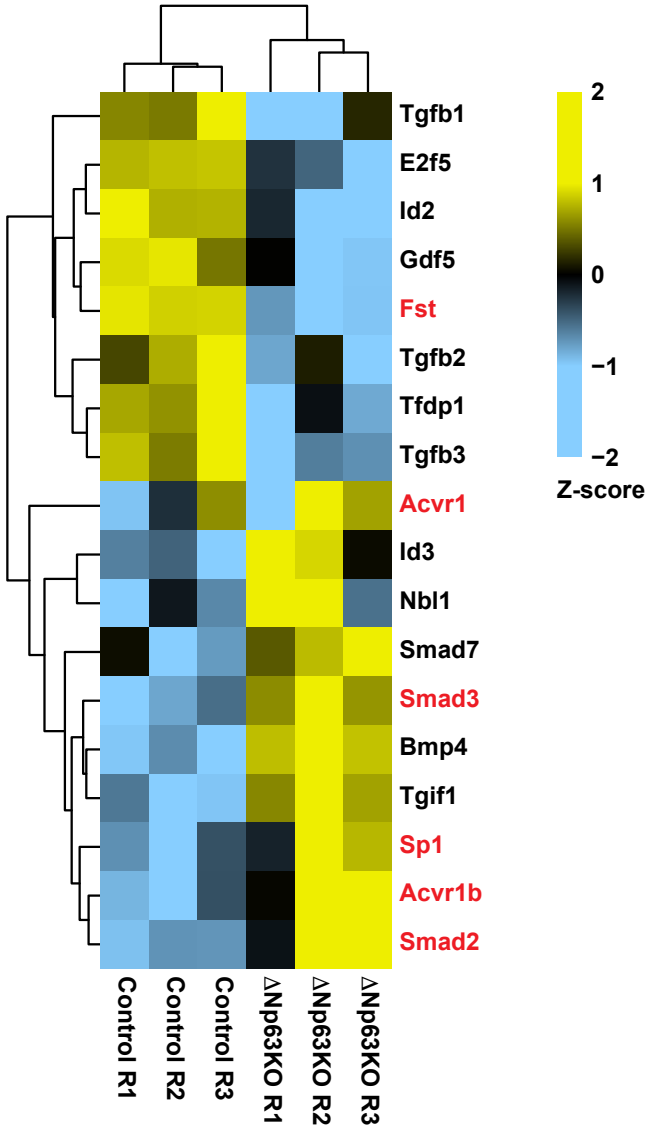

Figure S6. TGF-β Signaling Status in Control versus ΔNp63KO Mice. Related to Figure 2.

Heatmap visualization of select genes involved in TGF-β signaling in control compared to KO glands. Genes highlighted in red are involved in Activin signaling.

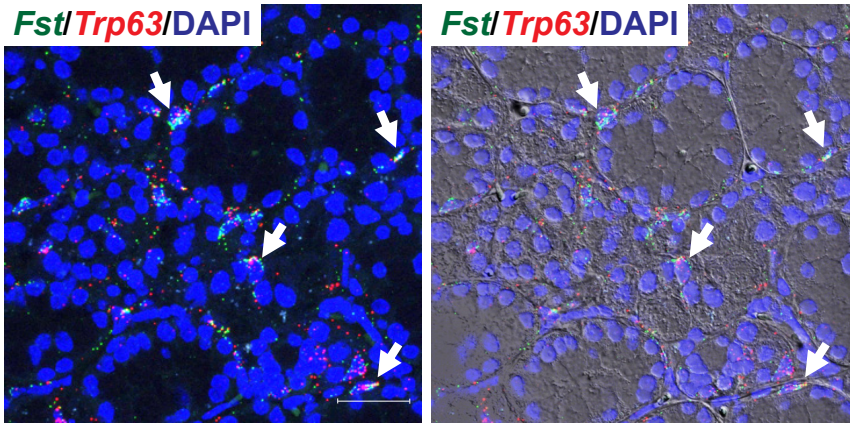

Figure S7. Expression Profile of *Trp63* and *Fst* in the adult mouse SMG. Related to Figure 5. *Trp63* and *Fst* mRNA transcripts were visualized in adult male SMGs using RNAscope® analysis (left panel). Right panel shows immunofluorescence image in left panel with Differential Interference Contrast (DIC). White arrows indicate cells which co-express both ΔNp63 and *Fst* mRNA transcripts. Scale bar: 18.75μm.

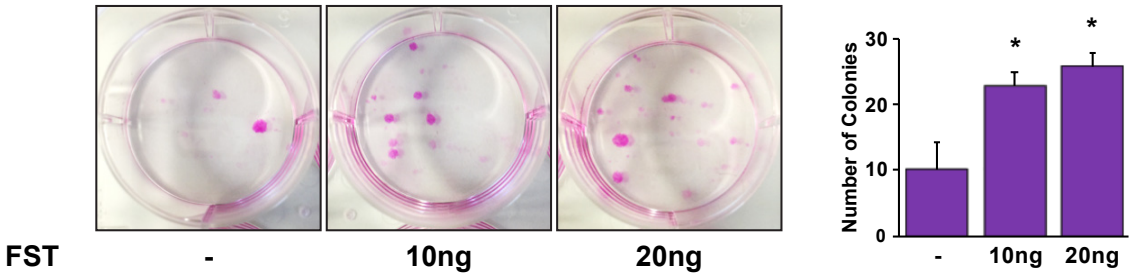

Figure S8. Fst Maintains the Clonogenic Potential of pSEPCs. Related to Figure 6. Representative images of Rhodamine B staining of wild type pSEPCs clones treated with increasing concentrations of Fst. Right panel is a quantification of the number of colonies formed after 14 days based on the concentration of Fst as indicated. Data are represented as ± S.D (n=3). $^{*}p<0.05$

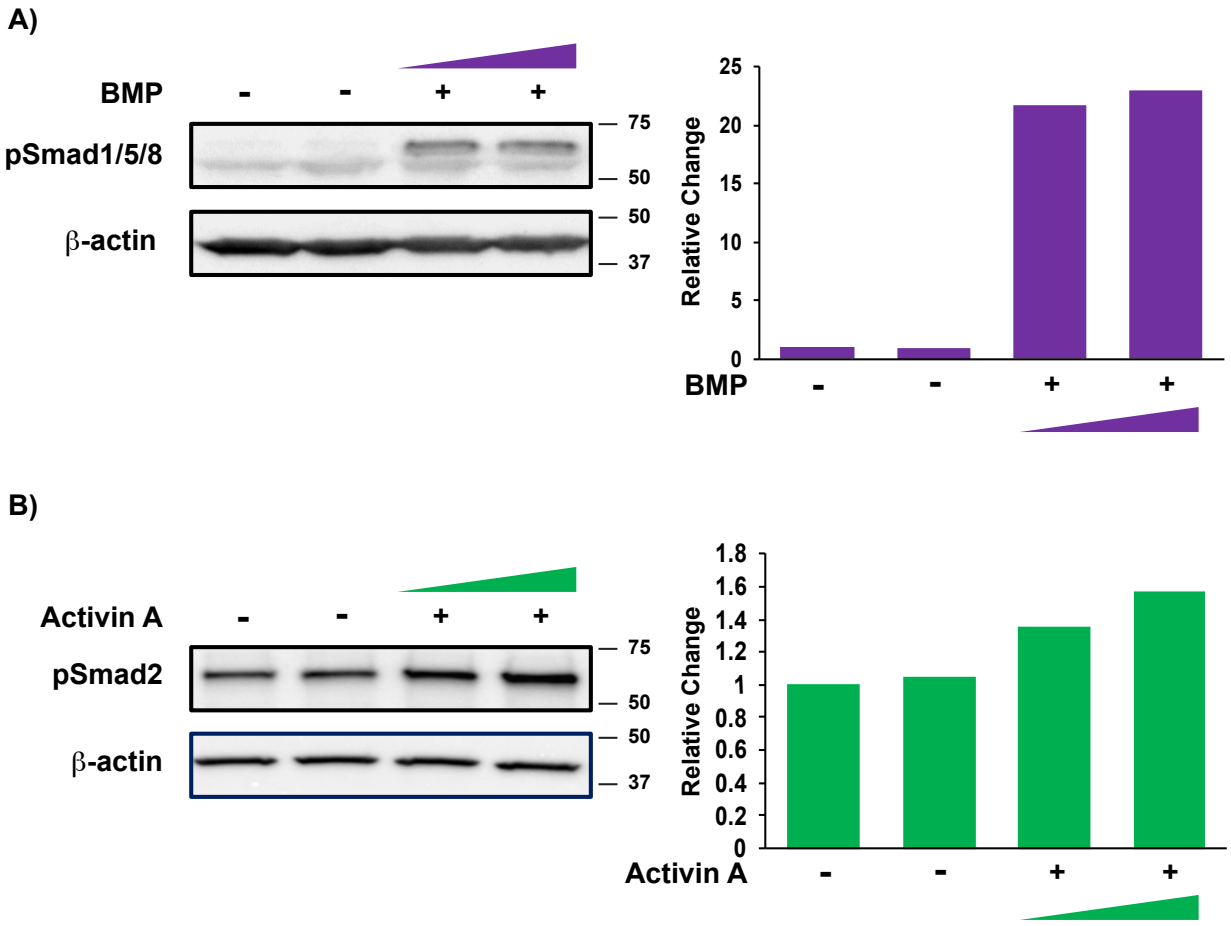

Figure S9. Status of TGF-β Signaling in pSEPCs. Related to Figure 6. (A) Western blot analysis demonstrating the status of BMP signaling in pSEPCs. In the absence of BMP, pSMAD1/5/8 is not detected. Conversely, upon the addition of increasing concentrations of BMP, pSMAD1/5/8 is detected. A quantification of pSMAD1/5/8 levels is shown on the right. pSMAD1/5/8 levels were normalized to β-actin. (B) Western blot shows Smad2 phosphorylation in the absence of Activin A, suggesting this signaling pathway is active in these cells. Treatment with Activin A results in increased pSmad2 levels. Quantification of pSMAD2 levels is shown on the right. pSMAD2 levels were normalized to β-actin.

Transparent Methods

Mice

All animal experiments and procedures were performed in accordance with the State University of New York at Buffalo (University at Buffalo) Institutional Animal Care and Use Committee (IACUC) regulations. All procedures were approved by University at Buffalo IACUC. The following mice were purchased from The Jackson Laboratory (Bar Harbor, Maine): Wild type C57BL/6J (Stock No. 000664) and UBC^{CreERT2} (B6.Cg-Ndor1$^{Tg(UBC-cre/ERT2)1Ejb}$/1J; Stock No. 007001). The ΔNp63-floxed (ΔNp63$^{fl/fl}$) mice were provided from Elsa Flores and have been described previously (Chakravarti et al., 2014). Establishment of the Trp63^{CreERT2} mice have been previously reported (Lee et al., 2014).

METHOD DETAILS

Conditional Deletion of ΔNp63 in Adult Mice.

Working stock of tamoxifen solution was prepared by dissolving 10mg of inactive form of tamoxifen (Sigma) in 1ml of corn oil by rocking at 55°C. A 200µl dose of tamoxifen was administered to 10- to 12-week old mice male and female *UBC^{CreERT2};ΔNp63$^{fl/fl}$*, *Trp^{CreERT2};ΔNp63$^{fl/fl}$* or *ΔNp63$^{fl/fl}$* mice by intraperitoneal (IP) injection. A second IP injection of tamoxifen in corn oil was administered three days later. Mice were euthanized by CO_2 inhalation and submandibular glands were harvested.

Immunostaining and Imaging

Harvested submandibular glands were fixed in 10% Neutral Buffered Formalin solution at room temperature. Fixed glands were processed, paraffin embedded, and sectioned to 5µm thickness. Paraffin embedded submandibular gland tissue sections were deparaffinized for immunofluorescence analysis as previously described (Rizzo et al., 2016). Antigen retrieval was

performed with sodium citrate buffer (pH 6) and the sections were blocked with M.O.M kit (Vector labs). Primary antibodies used at the indicated dilutions include alpha-smooth muscle actin (SMA) (1:200, Sigma, 1A4), Amy1 (1:100, BosterBio), Aqp5 (1:100, Alomone Labs), Cleaved Caspase-3 (1:100, Cell Signaling Technology, D175), K5 (1:100, gift from Dr. Julie Segre), K7 (1:50, Abcam), K14 (1:100(Rizzo et al., 2016)), Ki67 (1:100, Leica Biosystems, MM1), Mist1 (1:100, Abcam), Muc10 (1:100, Everest Biotech), Nkcc1 (1:100, Santa Cruz Biotechnology), ΔNp63 (1:25)(Romano et al., 2006), p63 (1:25, Biocare Medical, 4A4), p63 (1:25, Cell Signaling Technology, D2K8X), Troma-III (1:50, Development Studies Hybridoma Bank). Sections were mounted using VECTASHIELD Antifade Mounting Medium with DAPI (Vector Laboratories) and imaged using a ZEISS LSM 510 Meta Confocal microscope with ZEISS ZEN Black imaging software.

Ductal-to-Acini Ratio Quantification

The areas of acini and ducts were measured with ImageJ and were converted into ratios. Approximately 9 fields of view (100x) were used for each quantification analysis. Values are reported as mean ± standard deviation (S.D.).

Saliva Collection

Mouse saliva was collected for 10 minutes following an intraperitoneal injection with pilocarpine HCl (0.3mg/100µl, Sigma-Aldrich). Saliva was centrifuged briefly and measured by pipette.

Generating Single Cell Suspensions

Ten to 12-week old control and tamoxifen administered female mice were euthanized by CO_2 inhalation. Single cell suspensions were generated from excised submandibular glands by mechanical and enzymatic digestion. The glands were minced with scissors and were incubated in 0.125% Trypsin in DMEM/F12 supplemented with 0.5mg/ml Collagenase II (Gibco) and 0.5mg/ml Dispase II (Roche) rocking at 125 rpm for 40 minutes at 37°C. The suspension was

centrifuges at 400xg for 10 minutes and the supernatant was discarded. The tissue was resuspended with 0.125% Trypsin in DMEM/F12 supplemented with 0.5ml Collagenase II and 10Units/µl DNase I (Zymo research). The tissue suspension was further digested for 20 minutes by rocking at 125 rpm for 20 minutes. Trypsin and collagenase II were inactivated with cold 10% FBS in DMEM/F12. Cell suspension was filtered through 40µm nylon filter and was resuspended with CELLnTEC (CnT) media. Cells were confirmed to be in single cell suspensions by direct microscopic observation, prior to use in downstream applications including scRNA-seq, FACS Analysis, Clonogenic Assays and 3D Spheroid Cultures.

Clonogenic Assay

Single cells were seeded at a density of $5 \cdot 10^5$ cells/well on non-coated plastic 6-well plates in CnT media. Cells were cultured at 37°C in 5% CO_2 for 14 days and were fixed for 2 hours with 4% paraformaldehyde (PFA). Fixed colonies were stained for 1 hour with 2% Rhodamine B in distilled water (Sigma catalog no. R6626, St. Louis, MO) and was rinsed several times with tap water to visualize individual colonies. Only colonies which consisted of at least 50 cells were selected for quantification.

3D Spheroid Cultures on Matrigel

One hundred microliters of matrigel (BD Biosciences) (2:1 of matrigel to CnT media) was allowed to solidify in a 37°C incubator in 5% CO_2 for 1 hour in 8-well chambers mounted on No. 1.5 German borosilicate coverglass (Nalge Nunc International, Naperville, IL). Upon solidification, 5,000 single cells/well were seeded on the matrigel in CnT media. 3D-spheroids were grown at 37°C in 5% CO_2.

Single-cell RNA Sequencing Analysis

Single cell suspensions from freshly isolated adult female control and ΔNp63KO murine SMG were generated for scRNA-seq analysis as previously described (Song et al., 2018, Oyelakin et

al., 2019). A total of 1970 control cells were sequenced to a depth of 35,984 reads per cell and 1,123 median genes per cell. A total of 4720 ΔNp63KO cells were sequenced to a depth of 15,964 reads per cell and 740 median genes per cell. The output from 10X Genomics Cellranger version 2.0.2 pipeline was used as input into the R analysis package Seurat version 3.1.1 (Stuart et al., 2019). Cells with high unique molecular index counts (nCount_RNA > 12000), and low gene detection rates (nFeature_RNA<200), high mitochondrial transcript load (>80%), and high transcript counts for red blood cell markers were filtered from the analysis. After filtering and down-sampling to control for variable cell capture efficiencies on the 10X platform, a total of 1828 cells per sample were analyzed. The data was normalized using Seurat's SCTransform version 0.2.0. Principle component analysis (PCA) and UMAP (Uniform Manifold Approximation and Projection) algorithm was used for dimensionality reduction and visualization, followed by the construction of a SNN (Shared Nearest Neighbor) graph and clustering analysis. Using the called clusters, cluster-to-cluster differential expression testing using the Wilcoxon Rank Sum identified unique gene markers for each cluster. A complete list of differentially expressed genes are provided in Table S2 and S3. Datasets have been deposited in the Gene Expression Omnibus (GEO) database under the accession number GEO: GSE145268.

RNA Sequencing Analysis

Total RNA was extracted from whole mouse salivary gland tissues as previously described (Gluck et al., 2016). For each RNA sample, 50bp cDNA-libraries were generated using the TrueSeq RNA Sample Preparation Kit (Illumina). Libraries were single-end sequenced on the Illumina HiSeq 2500. Quality metrics were generated using FASTQC (Andrews, 2010) v0.4.3, and high quality reads were mapped to the Mus musculus genome (mm9 build) with the Tophat2 (Kim et al., 2013) v2.0.13 wrapper for Bowtie2 (Langmead and Salzberg, 2012) v2.2.6. The reads that aligned to the mouse genome were counted using featureCounts (Liao et al., 2014). All computational analysis was performed on the R Statistical Platform (R Development Core Team, 2018) v 3.5.1.,

heatmaps were generated using Pretty Heatmaps Package (Kolde, 2019), and differential gene expression analysis was performed using DESeq2 package (Love et al., 2014) v1.22.2. All differentially expressed genes were called at a log2 Fold Change of 1 and an adjusted *p*-value of 0.1 unless otherwise specified. A complete list of differentially expressed genes in control and ΔNp63KO SMGs are provided in Table S1. Datasets have been deposited in the Gene Expression Omnibus (GEO) database under the accession number GEO: GSE145268.

Chromatin Immunoprecipitation, Sequencing Analysis and qPCR validation

ChIP-seq experiments were performed as previously described (Gluck et al., 2019, Sethi et al., 2017). Briefly, pSEPCs were grown to ~90% confluency and cross-linked with 1% Formaldehyde for 10 minutes. Lysates from the fixed cells were subsequently sonicated with a Diagenode Bioruptor to obtain sheared chromatin with an approximate fragment length of 150–400 bp. The ChIP was carried out using 2 µg of the anti-p63, mouse IgG control or anti-H3K27Ac antibodies. Libraries from ChIP DNA and input controls were then subjected to 50 bp single-end sequencing on an Illumina HiSeq 2500, which resulted in 15–25 million reads per sample. The raw ChIP-sequencing reads were mapped to the Mus musculus genome (mm9 build) using Bowtie v1.1.1. All ChIP-seq experiments underwent strand cross-correlation analysis using SPP v1.10.1 and deemed acceptable if the QualityTag score was 1 or higher, as previously described (Gluck et al., 2019, Sethi et al., 2017). Trp63 peaks were identified using MACS2 v2.1.0. Narrow-Peaks from H3K27Ac ChIP-seq were called using MACS2 v2.1.0 using the following parameters (-p 0.1 –nomodel–extsize 150). All identified peaks were matched to the nearest gene using GREAT analysis using default settings. ChIP-Seq Signal was visualized using the deeptools program. Briefly, ChIP signal was converted to RPKMs (Reads per Kilobase per Million Mapped Reads) and was subsequently summed across the genome within 10 base-pair bins at the selected loci. ChIPed DNA from anti-p63, mouse IgG control was used for real-time qPCR to validate binding to the *Fst* genomic locus.

RNA Isolation and Quantitative RT-PCR

Total RNA from the single cell suspensions was isolated and purified using TRIzol (Invitrogen) according to established protocols. Two micrograms of total RNA from mSG cells grown in culture or spheres was reverse transcribed using the iScript cDNA Synthesis Kit (Bio-Rad) according to the manufacturer's instructions. Quantitative real-time RT-PCR was performed on an iCycler iQ PCR machine using iQ SYBR Green Supermix (Bio-Rad). All quantitative real-time RT-PCR assays were performed in triplicate in at least three independent experiments. Relative expression values of each target gene were normalized to hypoxanthine guanine phosphoribosyltransferase (Hprt) expression.

Fluorescence-activated Cell Sorting Analysis

10^6 cells/tube of single cell suspension was resuspended in FACS buffer (1% BSA in HBSS). The cells were blocked with anti-CD16/CD32 FccIII/II receptor antibody (BD Pharmingen) and stained with CD24-PE (BD Biosciences, clone M1/69, 1:1000) and CD29-APC (eBioscience, clone HMb1-1, 1:1000). The cells were stained with Ghost Dye Violet 510 (Tonbo Biosciences, 1:1000) to measure for cell viability. To determine non-specific background staining, single cells were stained with PE Rat IgG (BD Pharmingen, 1:1000) or APC Armenian Hamster IgG (Invitrogen, 1:1000) as isotype control. The data acquisition of stained cells was performed using a SORP Fortessa equipped with FACSDiva software and the analysis was performed with FlowJo v.10 (Tree Star).

Protein Extraction and Western Blot Analysis.

Single cells were seeded at a density of 10^6 cells/well on non-coated plastic 6-well plates in CnT media. Cells were cultured at 37°C in 5% CO_2 for ten days. Cells were treated with 20ng/ml Fst, 10ng/ml Activin A, or both for 2 hours. For conditional knockdown of ΔNp63, 1μM of activated tamoxifen ((Z)-4-Hydroxytamoxifen, 4-OHT, Sigma-Aldrich) was added to CnT media on the eighth day of culture. After 72 hour incubation in 4-OHT, the cells were either harvested or were

treated with 20ng/ml Fst, 10ng/ml Activin A, or both for additional 2 hours. Cultured pSEPCs were harvested and proteins were extracted from cultured primary epithelial cells in RIPA buffer containing 2μg/ml phosphatase and protease inhibitor cocktail. Antibodies were diluted in 5% milk in TBST. Primary antibodies used were p63α (1:10000, Cell Signaling Technology, D2K8X), Fst (1:10000, Abcam), Smad2/3(1:10000, Cell Signaling Technology), Phospho-Smad2(1:10000, Cell Signaling Technology), β-actin(1:10000, Cell Signaling Technology, 13E5). The blot was stripped three times using stripping buffer (Thermo Fisher) and was re-probed with β-actin for normalization. n=3

RNAscope® Fluorescence *in situ* Hybridization

FISH was performed using the RNAscope® Multiplex Fluorescent Detection Kit v2 according to manufacturer's protocol on formalin fixed paraffin embedded (FFPE) sections. Tissue sections of 5μm thickness of 12-week adult mouse salivary glands were used to probe for p63 and Fst. Opal 520 (1:1500) and Opal 570 (1:1000) fluorescent dye were used for visualization of Fst and p63 mRNA, respectively. The sections were counterstained with DAPI, mounted using VECTASHIELD Antifade Mounting Medium, and imaged using a ZEISS LSM 510 Meta confocal microscope with ZEISS ZEN Black imaging software.

QUANTIFICATION AND STATISTICAL ANALYSIS

Statistical analyses

Quantified results were reported as mean ± standard deviation (S.D.) of at least three or more independent experiments. Data comparison between control and KO groups were performed with one-sided Student's t-test with false discovery rate of less than 5%.

Key Resources Table

REAGENT or RESOURCE	SOURCE	IDENTIFIER
Antibodies		
Mouse anti-Actin, α-Smooth Muscle	Sigma-Aldrich	A2547; RRID:AB_476701
Rabbit anti-Alpha Amylase 1	BosterBio	PA1486
Rabbit anti-Aquaporin 5	Alomone Labs	AQP-005; RRID:AB_2039736
Rabbit anti-Cleaved Caspase 3	Cell Signaling	9661; RRID:AB_2341188
Rabbit anti-Krt5	Gift from Julie Segre	N/A
Mouse anti-Cytokeratin 7	Abcam	ab9021; RRID:AB_306947
Guinea Pig anti-Krt14	(Rizzo et al., 2016)	N/A
Mouse anti-Ki67	Leica Biosystems	NCL-Ki67-MM1; RRID:AB_442101
Rabbit anti-Mist1	Abcam	ab187978
Goat anti-Muc10	Everest Biotech	EB10617
Goat anti-Nkcc1	Santa Cruz Biotechnology	sc-21545; RRID:AB_2188633
Rabbit anti-ΔNp63 (RR14)	(Romano et al., 2006)	N/A
Rabbit anti-p63α	Cell Signaling	13109; RRID:AB_2637091
Mouse anti-p63	Biocare Medical	CM 163 A, B, C; RRID:AB_10582730
Rat anti-Troma III	Development Studies Hybridoma Bank	http://dshb.biology.uiowa.edu/; RRID:AB_2133570
Mouse Anti-Mucin 13	Santa Cruz Biotechnology	sc-373857; RRID:AB_10990901
H3K27Ac Antibody	Diagenode	C15410174; RRID:AB_2716835
Purified Rat Anti-Mouse CD16/CD32 (Mouse BD Fc Block™)	BD Pharmingen	553143; RRID:AB_394658
PE Rat Anti-Mouse CD24	BD Pharmingen	561079; RRID:AB_2034001

PE Rat IgG2b, κ Isotype Control	BD Pharmingen	553989; RRID:AB_10049479
Anti-Mouse/Rat CD29 (Integrin beta 1) APC	eBioscience	17-0291; RRID:AB_1210794
Armenian Hamster IgG Isotype Control, APC, eBioscience™	Invitrogen	17-4888-81; RRID:AB_470191
Ghost Dye™ Violet 510	Tonbo Biosciences	13-0870
Rabbit anti-Follistatin	Abcam	ab157471
Rabbit anti-Smad2/3	Cell Signaling	8685; RRID:AB_10889933
Rabbit anti-Smad2 (phospho Ser465/Ser467)	GeneTex	GTX133614
Recombinant Human/Mouse/Rat Activin A Protein	R&D Systems	338-AC
Recombinant Human Follistatin 300	R&D Systems	669-FO
Rabbit anti-β-actin	Cell Signaling	4970; RRID:AB_2223172
Donkey anti-Rabbit IgG (H+L) Highly Cross-Adsorbed Secondary Antibody, Alexa Fluor 488	Invitrogen	A-21206; RRID:AB_2535792
Donkey anti-Goat IgG (H+L) Cross-Adsorbed Secondary Antibody, Alexa Fluor 488	Invitrogen	A-11055; RRID:AB_2534102
Goat anti-Rat IgG (H+L) Cross-Adsorbed Secondary Antibody, Alexa Fluor 568	Invitrogen	A-11077; RRID:AB_2534121
Goat anti-Guinea Pig IgG (H+L) Highly Cross-Adsorbed Secondary Antibody, Alexa Fluor 568	Invitrogen	A-11075; RRID:AB_2534119
Donkey anti-Rabbit IgG (H+L) Highly Cross-Adsorbed Secondary Antibody, Alexa Fluor 568	Invitrogen	A-10042; RRID:AB_2534017
Donkey anti-Mouse IgG (H+L) Highly Cross-Adsorbed Secondary Antibody, Alexa Fluor 488	Invitrogen	A-21202; RRID:AB_141607
Chemicals, Peptides, and Recombinant Proteins		
Tamoxifen	Sigma-Aldrich	T5648
(Z)-4-Hydroxytamoxifen	Sigma-Aldrich	H7904
Histo-Clear II	National Diagnostics	HS-202
Eosin Y solution, aqueous	Sigma-Aldrich	HT110216
Hematoxylin Solution, Harris Modified	Sigma-Aldrich	HHS16
Matrigel™	Corning	356231
Rhodamine B	Sigma-Aldrich	R6626

TRIzol™ Reagent	Invitrogen	15596018
Bovine Serum Albumin Fraction V, heat shock	Roche	03116956001
DirectPCR Lysis Reagent (Tail)	Viagen Biotech	102-T
Collagenase, Type II, powder	Gibco	17101015
Dispase II (neutral protease, grade II)	Roche	4942078001
DNase I	Zymo Research	E1009
Restore™ Western Blot Stripping Buffer	Thermo Fisher Scientific	21063
Critical Commercial Assays		
Mouse on Mouse (M.O.M.) Basic Kit	Vector Laboratories	BMK-2202
iQ™ SYBR® Green Supermix	Bio-Rad	1708882
iScript™ cDNA Synthesis Kit	Bio-Rad	1708890
TruSeq RNA Library Prep Kit	Illumina	RS-122-2001
ChIP-IT High Sensitivity® Kit	Active Motif	53040
ThruPLEX® DNA-Seq Kit	Rubicon Genomics	R400674
RNAscope® Multiplex Fluorescent Detection Kit v2	Advanced Cell Diagnostics	323110
RNAscope® Probe Diluent	Advanced Cell Diagnostics	300041
RNAscope® Probe - Mm-Fst	Advanced Cell Diagnostics	454331
RNAscope® Probe - Mm-Trp63-C2	Advanced Cell Diagnostics	464591-C2
Opal 520 Reagent Pack	Akoya Biosciences	FP1487001KT
Opal 570 Reagent Pack	Akoya Biosciences	FP1488001KT
Deposited Data		
RNA sequencing data	This paper	GEO:GSE145268
scRNA sequencing data	This paper	GEO:GSE145268
p63 ChIP sequencing data	This paper	GEO:GSE145268
H3K27Ac ChIP sequencing data	This paper	GEO:GSE145268
Experimental Models: Organisms/Strains		
Mouse: B6.Cg-Ndor1$^{Tg(UBC-cre/ERT2)1Ejb/1J}$	Jackson Laboratory	007001; RRID:IMSR_JAX:007001

Mouse: C57BL/6J	Jackson Laboratory	000664; RRID:IMSR_JAX:000664
Mouse: $\Delta Np63^{fl/fl}$	Gifted (Chakravarti et al., 2014)	N/A
Mouse: $Trp63^{CreERT2}$	Gifted (Lee et al., 2014)	N/A
Oligonucleotides		
Genotyping primers: Cre (F): 5'-GAG TGA TGA GGT TCG CAA GA-3'	Integrated DNA Technologies	N/A
Genotyping primers: Cre (R): 5'-CTC CAC CAG AGA CGG AAA TC-3'	Integrated DNA Technologies	N/A
Genotyping primers: ΔNp63 floxed (F): 5'-ACA GTC CTC TGC TTT CAG C-3'	Integrated DNA Technologies	N/A
Genotyping primers: ΔNp63 floxed (R): 5'-TTC ACA TTC ACA CAG ACA GCT CC-3'	Integrated DNA Technologies	N/A
Genotyping primers: ΔNp63 Knockout (F): 5'-TAC TTT CAA ACA GCT ATT CTC AGG-3'	Integrated DNA Technologies	N/A
Genotyping primers: ΔNp63 Knockout (R): 5'-CAC ACA GCA CTG GCC TTG C-3'	Integrated DNA Technologies	N/A
qRT-PCR primers: ΔNp63 (F): 5'-TGC CCA GAC TCA ATT TAG TGA GC-3'	Integrated DNA Technologies	N/A
qRT-PCR primers: ΔNp63 (R): 5'-GAC GAG GAG CCG TTC TGA ATC-3'	Integrated DNA Technologies	N/A
qRT-PCR primers: Krt5 (F): 5'-GGA ACG AAT CCC AAC CTC TG-3'	Integrated DNA Technologies	N/A
qRT-PCR primers: Krt5 (R): 5'-CAT TTT GGG GTC TGG GTC AC-3'	Integrated DNA Technologies	N/A
qRT-PCR primers: Krt14 (F): 5'-GTC TGC TGG AGG GAG AGG AC-3'	Integrated DNA Technologies	N/A
qRT-PCR primers: Krt14 (R): 5'-GGA TCT GGC GGT TGG TGG AG-3'	Integrated DNA Technologies	N/A
qRT-PCR primers: Acta2 (F): 5'-GAC GGG CAG GTG ATC ACC ATT G-3'	Integrated DNA Technologies	N/A

qRT-PCR primers: Acta2 (R): 5'-GTT TCG TGG ATG CCC GCT GAC-3'	Integrated DNA Technologies	N/A
qRT-PCR primers: Krt18 (F): 5'-CTG GTC TCT CGC TTC GCT CTC-3'	Integrated DNA Technologies	N/A
qRT-PCR primers: Krt18 (R): 5'-AGC CCA GGG ACC GGT AGT TG-3'	Integrated DNA Technologies	N/A
qRT-PCR primers: Krt19 (F): 5'-CTG CGT CCC TTT TTC CTT CG-3'	Integrated DNA Technologies	N/A
qRT-PCR primers: Krt19 (R): 5'-CTG ACC CAA TGC GTA CTG AAC-3'	Integrated DNA Technologies	N/A
qRT-PCR primers: Acvr1b (F): 5'-ACC AAA CGA TAC ATG GCT CC-3'	Integrated DNA Technologies	N/A
qRT-PCR primers: Acvr1b (R): 5'-ATC TTC GTG CAA TCT CCC AG-3'	Integrated DNA Technologies	N/A
qRT-PCR primers: Fst (F): 5'-GAC AGT AAG TCG GAT GAG CC-3'	Integrated DNA Technologies	N/A
qRT-PCR primers: Fst (R): 5'-TTC TTC CGA GAT GGA GTT GC-3'	Integrated DNA Technologies	N/A
qRT-PCR primers: Fgf1 (F): 5'-TAC CCA CTG CAT GCT CTT TC-3'	Integrated DNA Technologies	N/A
qRT-PCR primers: Fgf1 (R): 5'-ATT TGT GCG GTT CTG GTA GG-3'	Integrated DNA Technologies	N/A
qRT-PCR primers: Fgf9 (F): 5'-CCA GAG AAA CAG CCG ATT AC-3'	Integrated DNA Technologies	N/A
qRT-PCR primers: Fgf9 (R): 5'-ATC AAC CAG GAG ACA CTA GG-3'	Integrated DNA Technologies	N/A
qRT-PCR primers: Csnk1e (F): 5'-AGG TTG AAG CAT GGA GTT GC-3'	Integrated DNA Technologies	N/A
qRT-PCR primers: Csnk1e (R): 5'-GGG GAT GTT TCG TCT TCA CA-3'	Integrated DNA Technologies	N/A

qRT-PCR primers: Id2 (F): 5'-TTC ACC AGG AGA ACA CGT TG-3'	Integrated DNA Technologies	N/A
qRT-PCR primers: Id2 (R): 5'-TCC AAC TGT AGA AAG GGC AC-3'	Integrated DNA Technologies	N/A
qRT-PCR primers: Kcnma1 (F): 5'-TAT CTC TCC AGT GCC TTC GT-3'	Integrated DNA Technologies	N/A
qRT-PCR primers: Kcnma1 (R): 5'-TGG CAG ACT TGT ACT CAA TGG-3'	Integrated DNA Technologies	N/A
qRT-PCR primers: Hprt (F): 5'-CCT CAT GGA CTG ATT ATG GAC AG-3'	Integrated DNA Technologies	N/A
qRT-PCR primers: Hprt (R): 5'-TCA GCA AAG AAC TTA TAG CCC C-3'	Integrated DNA Technologies	N/A
Software and Algorithms		
ZEN imaging software	Zeiss	https://www.zeiss.com/microscopy/us/products/microscope-software/zen.html
ImageJ	ImageJ	https://imagej.net/Downloads
Adobe Illustrator	Adobe	www.adobe.com
FlowJo v.10	TreeStar	https://www.flowjo.com/solutions/flowjo/downloads
CFX Manager	Bio-Rad	1845000
Image Lab	Bio-Rad	1709690
Cytoscape v.3.5.0	(Shannon et al., 2003)	https://cytoscape.org
ClueGO v.2.5.4	(Bindea et al., 2009)	http://apps.cytoscape.org/apps/cluego
Cellranger v.2.0.2	(Zheng et al., 2017)	https://support.10xgenomics.com/single-cell-gene-expression/software/overview/welcome
Seurat v3.1.1	(Stuart et al., 2019)	https://github.com/satijalab/seurat

FastQC (v. 0.4.3)	(Andrews, 2010)	https://www.bioinformatics.babraham.ac.uk/projects/fastqc/
Tophat2 v.2.0.13	(Kim et al., 2013)	https://ccb.jhu.edu/software/tophat
Bowtie2 v.2.2.6	(Langmead and Salzberg, 2012)	http://bowtie-bio.sourceforge.net/index
FeatureCount	(Liao et al., 2014)	http://bioinf.wehi.edu.au/featureCounts/
DESeq2 v.1.22.2	(Love et al., 2014)	http://bioconductor.org/packages/release/bioc/html/DESeq2
R v.3.5.1	The R Project for Statistical Computing	https://www.r-project.org/
RStudio v1.2.1335	The R Project for Statistical Computing	https://www.r-project.org
Other		
Corn oil	Sigma-Aldrich	C8267
Ethanol, Pure + Denatured 200 Proof	Decon Labs	2716
Ethanol, 190 Proof	Decon Labs	2801
VECTASHIELD® Antifade Mounting Medium with DAPI	Vector Laboratories	H-1200
Nunc™ Lab-Tek™ II Chambered Coverglass	Thermo Fisher Scientific	155409
CnT-Prime, Epithelial Culture Medium	CELLnTEC	CnT-PR
Penicillin-Streptomycin (10,000 U/mL)	Gibco	15140122
DMEM/F-12, HEPES	Gibco	11330032
HBSS	Gibco	14175095
Falcon® Cell Strainers (40μm)	Corning	352340

References

ANDREWS, S. 2010. FastQC: a quality control tool for high throughput sequence data.

BINDEA, G., MLECNIK, B., HACKL, H., CHAROENTONG, P., TOSOLINI, M., KIRILOVSKY, A., FRIDMAN, W. H., PAGES, F., TRAJANOSKI, Z. & GALON, J. 2009. ClueGO: a Cytoscape plug-in to decipher functionally grouped gene ontology and pathway annotation networks. *Bioinformatics,* 25**,** 1091-3.

CHAKRAVARTI, D., SU, X., CHO, M. S., BUI, N. H., COARFA, C., VENKATANARAYAN, A., BENHAM, A. L., FLORES GONZALEZ, R. E., ALANA, J., XIAO, W., LEUNG, M. L., VIN, H., CHAN, I. L., AQUINO, A., MULLER, N., WANG, H., COONEY, A. J., PARKER-THORNBURG, J., TSAI, K. Y., GUNARATNE, P. H. & FLORES, E. R. 2014. Induced multipotency in adult keratinocytes through down-regulation of DeltaNp63 or DGCR8. *Proc Natl Acad Sci U S A,* 111**,** E572-81.

GLUCK, C., GLATHAR, A., TSOMPANA, M., NOWAK, N., GARRETT-SINHA, L. A., BUCK, M. J. & SINHA, S. 2019. Molecular dissection of the oncogenic role of ETS1 in the mesenchymal subtypes of head and neck squamous cell carcinoma. *PLoS Genet,* 15**,** e1008250.

GLUCK, C., MIN, S., OYELAKIN, A., SMALLEY, K., SINHA, S. & ROMANO, R. A. 2016. RNA-seq based transcriptomic map reveals new insights into mouse salivary gland development and maturation. *BMC Genomics,* 17**,** 923.

KIM, D., PERTEA, G., TRAPNELL, C., PIMENTEL, H., KELLEY, R. & SALZBERG, S. L. 2013. TopHat2: accurate alignment of transcriptomes in the presence of insertions, deletions and gene fusions. *Genome Biol,* 14**,** R36.

KOLDE, R. 2019. Pretty Heatmaps.

LANGMEAD, B. & SALZBERG, S. L. 2012. Fast gapped-read alignment with Bowtie 2. *Nat Methods,* 9**,** 357-9.

LEE, D. K., LIU, Y., LIAO, L., WANG, F. & XU, J. 2014. The prostate basal cell (BC) heterogeneity and the p63-positive BC differentiation spectrum in mice. *Int J Biol Sci,* 10**,** 1007-17.

LIAO, Y., SMYTH, G. K. & SHI, W. 2014. featureCounts: an efficient general purpose program for assigning sequence reads to genomic features. *Bioinformatics,* 30**,** 923-30.

LOVE, M. I., HUBER, W. & ANDERS, S. 2014. Moderated estimation of fold change and dispersion for RNA-seq data with DESeq2. *Genome Biol,* 15**,** 550.

OYELAKIN, A., SONG, E. A. C., MIN, S., BARD, J. E., KANN, J. V., HORETH, E., SMALLEY, K., KRAMER, J. M., SINHA, S. & ROMANO, R. A. 2019. Transcriptomic and Single-Cell Analysis of the Murine Parotid Gland. *J Dent Res***,** 22034519882355.

R DEVELOPMENT CORE TEAM 2018. R: A Language and Environment for Statistical Computing. *R Foundation for Statistical Computing*.

RIZZO, J. M., OYELAKIN, A., MIN, S., SMALLEY, K., BARD, J., LUO, W., NYQUIST, J., GUTTMAN-YASSKY, E., YOSHIDA, T., DE BENEDETTO, A., BECK, L. A., SINHA, S. & ROMANO, R. A. 2016. DeltaNp63 regulates IL-33 and IL-31 signaling in atopic dermatitis. *Cell Death Differ*.

ROMANO, R. A., BIRKAYA, B. & SINHA, S. 2006. Defining the regulatory elements in the proximal promoter of DeltaNp63 in keratinocytes: Potential roles for Sp1/Sp3, NF-Y, and p63. *J Invest Dermatol,* 126**,** 1469-79.

SETHI, I., GLUCK, C., ZHOU, H., BUCK, M. J. & SINHA, S. 2017. Evolutionary re-wiring of p63 and the epigenomic regulatory landscape in keratinocytes and its potential implications on species-specific gene expression and phenotypes. *Nucleic Acids Res,* 45**,** 8208-8224.

SHANNON, P., MARKIEL, A., OZIER, O., BALIGA, N. S., WANG, J. T., RAMAGE, D., AMIN, N., SCHWIKOWSKI, B. & IDEKER, T. 2003. Cytoscape: a software environment for integrated models of biomolecular interaction networks. *Genome Res,* 13**,** 2498-504.

SONG, E. C., MIN, S., OYELAKIN, A., SMALLEY, K., BARD, J. E., LIAO, L., XU, J. & ROMANO, R. A. 2018. Genetic and scRNA-seq Analysis Reveals Distinct Cell Populations that Contribute to Salivary Gland Development and Maintenance. *Sci Rep,* 8**,** 14043.

STUART, T., BUTLER, A., HOFFMAN, P., HAFEMEISTER, C., PAPALEXI, E., MAUCK, W. M., 3RD, HAO, Y., STOECKIUS, M., SMIBERT, P. & SATIJA, R. 2019. Comprehensive Integration of Single-Cell Data. *Cell,* 177**,** 1888-1902 e21.

ZHENG, G. X., TERRY, J. M., BELGRADER, P., RYVKIN, P., BENT, Z. W., WILSON, R., ZIRALDO, S. B., WHEELER, T. D., MCDERMOTT, G. P., ZHU, J., GREGORY, M. T., SHUGA, J., MONTESCLAROS, L., UNDERWOOD, J. G., MASQUELIER, D. A., NISHIMURA, S. Y., SCHNALL-LEVIN, M., WYATT, P. W., HINDSON, C. M., BHARADWAJ, R., WONG, A., NESS, K. D., BEPPU, L. W., DEEG, H. J., MCFARLAND, C., LOEB, K. R., VALENTE, W. J., ERICSON, N. G., STEVENS, E. A., RADICH, J. P., MIKKELSEN, T. S., HINDSON, B. J. & BIELAS, J. H. 2017. Massively parallel digital transcriptional profiling of single cells. *Nat Commun,* 8**,** 14049.